Computer Modeling in
Engineering & Sciences

Tech Science Press

DOI: 10.32604/cmes.2023.028771

ARTICLE

Dynamical Analysis of the Stochastic COVID-19 Model Using Piecewise Differential Equation Technique

Yu-Ming Chu[1], **Sobia Sultana**[2], **Saima Rashid**[3,*] and **Mohammed Shaaf Alharthi**[4]

[1]Department of Mathematics, Huzhou University, Huzhou, 313000, China

[2]Department of Mathematics, Imam Mohammad Ibn Saud Islamic University, Riyadh, 12211, Saudi Arabia

[3]Department of Mathematics, Government College University, Faisalabad, 38000, Pakistan

[4]Department of Mathematics and Statistics, College of Science, Taif University, P.O.Box 11099, Taif, 21944, Saudi Arabia

*Corresponding Author: Saima Rashid. Email: saimarashid@gcuf.edu.pk

Received: 06 January 2023 Accepted: 20 March 2023 Published: 03 August 2023

ABSTRACT

Various data sets showing the prevalence of numerous viral diseases have demonstrated that the transmission is not truly homogeneous. Two examples are the spread of Spanish flu and COVID-19. The aim of this research is to develop a comprehensive nonlinear stochastic model having six cohorts relying on ordinary differential equations via piecewise fractional differential operators. Firstly, the strength number of the deterministic case is carried out. Then, for the stochastic model, we show that there is a critical number $\mathbb{R}_0^S$ that can predict virus persistence and infection eradication. Because of the peculiarity of this notion, an interesting way to ensure the existence and uniqueness of the global positive solution characterized by the stochastic COVID-19 model is established by creating a sequence of appropriate Lyapunov candidates. A detailed ergodic stationary distribution for the stochastic COVID-19 model is provided. Our findings demonstrate a piecewise numerical technique to generate simulation studies for these frameworks. The collected outcomes leave no doubt that this conception is a revolutionary doorway that will assist mankind in good perspective nature.

KEYWORDS

COVID-19 epidemic model; piecewise fractional differential operators; piecewise numerical scheme; extinction; ergodicity and stationary distribution

1 Introduction

Coronavirus disease 2019 is a contagious infection transmitted by the serious acute respiratory syndrome coronavirus 2 (SARS-CoV-2). Headaches, congestion, weariness, muscle aches, breathlessness, diminished appetite, taste and aroma are typical problems. Effects including bronchitis, multi-organ failure, chronic pulmonary disruption phenomenon, septicaemia, tachycardia, cardiogenic shock, thrombosis, cardiac arrest, convulsions, meningitis, dementia and Guillain Barré syndrome may occur in certain people [1]. The implantation phase might last anywhere from two to fourteen days.

The new coronavirus transmits through fluids created by inhaling, breathing or conversing. Liquids emitted by sick individuals are breathed into the trachea of others, developing quality infestations. If individuals contact infected materials and then their faces with unhygienic fingers after the particles tumble on them, they can transmit the disease. Whereas saliva and mucous are key infection transmitters, new evidence indicates that the infection is transferred via faecal contamination pathways. Aerosol-generating methods (AGMs) potentially assist in simpler pathogen propagation than standard pathogen propagation.

SARS-CoV-2 shares characteristics with the severe acute respiratory syndrome coronavirus (SARS-CoV or SARS-CoV1), an encapsulated, newly infected cause that primarily attacks the trachea after entering the host organism and binding to angiotensin-converting-enzyme 2 (ACE2), which is highly prevalent in atelectasis type II (AT2) keratinocytes of the respiratory system [2,3]. It is classified as a congenital illness since it is spread to people via bats as biological transmitters. According to chromosomal investigation, the infection belongs to the Betacoronavirus species and includes two bat-derived viruses [4].

COVID-19 was reported on December 31, 2019, in Wuhan, China's Hubei region, and has since proliferated globally. On January 30, 2020, the WHO labelled the epidemic a Public Health Emergency of International Concern (PHEIC), and on March 11, 2020, it designated the disease a global epidemic [4,5]. As of August 20, 2020, 217 nations and entities, such as Pakistan, had recorded 30.6 million documented infections and 890,000 fatalities. The very first COVID-19 incidence in Pakistan was detected on February 26, 2020. On September 20, 2020, the government had 306,304 documented favourable patients, 6420 fatalities, and 292,869 recovered [6].

COVID-19 has had a negative impact on the world's economic development, basic necessities, price volatility, cultural activities and entertainment domains, religious ceremonies, recreation, film, hospitality, academia, care facilities, and democracy. Several specifics about the spread, mitigation, and therapy of this novel ailment are being investigated by mathematicians and virologists [7–9]. Numerous studies using mathematical simulations to understand infection processes and epidemic interventions have been presented [10–14]. Tang et al. [15] developed a cohort system in which the community was classified into nine ordinary differential equations. Considering evidence from scientifically verified COVID-19 occurrences in central China during the month of January, they approximated the virus's fundamental reproductive rate. It was discovered that prevention strategies can successfully diminish the reproductive capacity. Tang et al. [16] examined a simplified form of their earlier approach, anticipating time-dependent interaction and identification outcomes. This resulted in a lower reproductive rate than had been forecasted in their prior investigation. Li et al. [17] discussed coronavirus dissemination utilizing an SEIR approach for the incidents reported in Wuhan as well as the proportion of exported infections. It is demonstrated that implementing preventive actions, including immigration prohibitions, might be critical in understanding epidemic patterns and the chances of controlling their dissemination. In [18], it seems to be other noteworthy research where the propagation speed is regarded to be a time-dependent variable. The structure is created by adding three additional compartments to the SEIR system. Other significant breakthroughs in innovative coronavirus modelling methodologies can be discovered in [19–24].

Scientists in numerous classifications and scientific disciplines have gravitated toward using fractional systems of differential equations (DEs) in the majority of their novel evidence and investigations as a consequence of the emergence of fractional derivatives [25–27]. In addition, to see this realistically, we can resort to numerical techniques of the proliferation and evolution of numerous infections and communicable conditions, which have emerged as an intriguing issue for scholars in past centuries, employing fractional frameworks of initial value problems. While reviewing the articles, we discovered that various scholars have proposed kernels that can be employed to create fractional differential formulations. The major motivation behind this is that serious challenges exhibit signs of mechanisms that are similar to the behaviours of precise scientific expressions. Fractional calculus incorporating a power law kernel is led by the contributions of Riemann, Liouville, Cauchy, and Abel. Caputo later improved their approach, and this form has been employed in several scientific disciplines owing to its capacity to enable classical initial conditions (ICs) [28]. Prabhakar proposed an appropriate kernel containing three components as a combo of index-law and the generalized Mittag-Leffler (GML) kernel [29–31]. This form has likewise piqued the interest of numerous scholars and investigations into both concepts and implementations have been conducted [32,33].

Furthermore, the various kernels have distinctive features; for instance, index-kernel only aids in the replication of systems that indicate index-kernel tendencies. GML, the combination of the index kernel and the generalized three distinct, has its own applicability domain [34]. Because the phenomenon is multifaceted, Caputo and Fabrizio developed a novel kernel, a particular exponential kernel exhibiting Delta Dirac characteristics. A differential formulation that is becoming increasingly popular because of its capacity to repeat processes after fading memory [35–38]. Furthermore, the notion of fractional derivative having a nonsingular kernel was pioneered by this kernel, marking the inauguration of a revolutionary era in fractional calculus [39]. A scientist's observation regarding the kernel's non-fractionality resulted in the creation of a novel kernel, the GML function, including one component. Atangana et al. [40] proposed this formulation, which represents another advancement in the discipline of fractional calculus. The formulationsÂ have been employed successfully in a variety of fields of study. Glancing at reality and its intricacies, it is clear that these proposed kernels are insufficient to forecast all of our universe's complicated characteristics. Following the remark, one will look for a different kernel or modified kernel, or a set of procedures that will be used to add novel differential formulations. Sabatier has proposed various kernel variants that will additionally lead to novel avenues of inquiry [41]. In addition to these remarkable breakthroughs, numerous additional notions were proposed, such as the conception of short memory and the definition of a fractional derivative in the Caputo interpretation for distinct characteristics of fractional orders. Notwithstanding the well-known formulation, which takes a fractional order to be time-dependent, the goal is to achieve a different form of variable order derivative. Wu et al. [42] proposed and implemented this scenario in chaotic theory. However, researchers have discovered that some real-world phenomena demonstrate mechanisms exhibiting varying behaviours as a factor of space and time. A transition from deterministic to stochastic, either from index-law to exponential decay, is an example. Because conventional differential formulations may be incapable of accounting for these tendencies, piecewise differential/integral formulations were devised to cope with issues manifesting crossover phenomena [43]. The primary goal of this article is to present a detailed evaluation, potential implementations, strengths and shortcomings of these two notions.

Mathematical modelling is a critical technique for understanding the transmission of a contagious illness, making predictions, and developing prevention and extinction tactics. Inspired by the aforesaid research, we propose to construct a stochastic framework to examine the impact of quarantine and isolation in reducing the transmission of the coronavirus epidemic in Pakistan via the piecewise differential operators. Pakistan is an emerging nation in the midst of an economic, environmental, and strategic crisis. The region's health sector is indeed inefficient and faces several issues. Atangana et al. [44] recently proposed the notions of piecewise differential/integral formulations. This revolutionary notion may represent the direction of modelling, as we propose in this work a progressive frontier to analyze epidemiological challenges involving crossover behaviours. A COVID-19 model in Pakistan will be discussed in this presentation stochastically. We will presume that real world propagation reveals waves exhibiting diverse chaotic structures, classical, local/nonlocal, randomness and that a permutation depending on the aforementioned mechanisms can lead to various tendencies. Furthermore, the qualitative characteristics of the aforesaid model are displayed in terms of Brownian motion, such as the existence-uniqueness of the global positive solutions, ergodic stationary distribution, extinction and persistence of the epidemic.

The remainder of the article is organized as follows. Section 2 discusses the preliminaries, framework construction, which is constructed on a variety of assumptions. Then we analyze the strength number of the deterministic COVID-19 model. Section 3 investigates the existence-uniqueness of the global non-negative solution of a stochastic system and calculates the crucial parameter that can readily decide the extermination and permanence of the infection. We additionally show that an ergodic stationary distribution emerges in the stochastic COVID-19 model. Section 4 introduces several simulation studies to illustrate the conceptual framework and illustrate the impacts of environmental white noise. Section 5 describes the results and discussion related to numerical findings. To conclude this work, several findings and appendices are offered.

2 Model Configuration

Taking into account the underlying hypotheses (Fig. 1), we construct a quantitative framework to investigate the behaviors of six classifications of people: susceptible $\mathbf{S}(\mathbf{t})$, exposed $\mathbf{E}(\mathbf{t})$, quarantined $\mathbf{Q}(\mathbf{t})$, infected $\mathbf{I}(\mathbf{t})$, separated $\mathbf{J}(\mathbf{t})$, and recovered $\mathbf{R}(\mathbf{t})$.

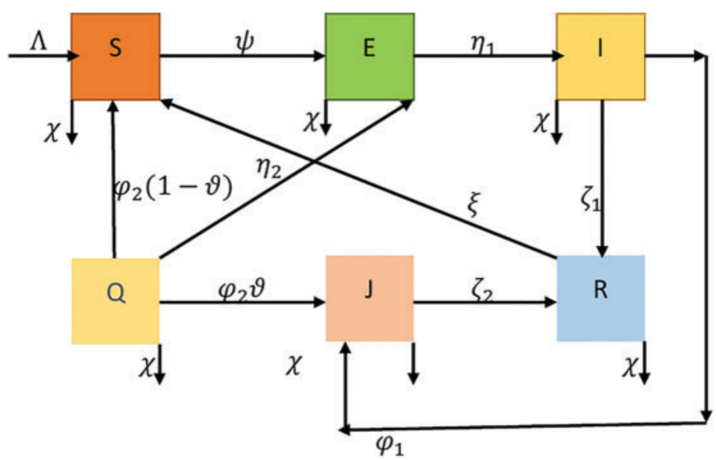

Figure 1: Schematic diagram of COVID-19 epidemic model

The vulnerable group expands by Λ due to consistent new recruits and a massive influx of people from the forced to evacuate and healed classifications at valuations of $\varphi_2(1-\vartheta)$, where $\vartheta \in (0, 1)$ is the proportion of people transmitted to the separated category due to therapeutic signs and symptoms, respectively. The vulnerable people get the virus and acquire transmitters at the pace ψ, causing a reduction in the vulnerable individual, which is additionally reduced by spontaneous mortality at the rate χ. The vulnerable people who have still not exhibited disease manifestations but are transmitters of the pathogen have boosted the number in the endangered category. The unprotected group is diminished at a pace of one by clinical manifestations η_1, two by isolation, and three by spontaneous mortality η_2.

The vulnerable people who have not yet manifested pathological changes but are susceptible to infection have increased the proportion of people in the η_2 classification. Random fatality reduces uncovered cohort seclusion by $\varphi_2\vartheta$, while initial symptoms reduce it by $\varphi_2(1-\vartheta)$.

People in the contaminated group acquire COVID-19 indications, resulting in an estimated prevalence. It diminishes at a rate of φ_1 due to quarantine of affected patients, recuperation at a rate ζ_1, and lingering death. People in the separated group have experienced COVID-19 indications and have been separated to receive healthcare attention. These people are drawn at φ_1 and $\varphi_2\vartheta$ rates from the infectious and confined categories, respectively. The segregated community shrinks as a consequence of the rate of ζ_1 recuperation and fatal disease. There is apparently no indication that people acquire lifetime sensitivity to COVID-19. As a result, it is expected that the restored people are vulnerable at a rate ξ. The populace grows at rates ζ_1 and ζ_2 due to the recovery of infectious and segregated people and shrinks due to spontaneous mortality.

The associated dynamic scheme of ordinary DEs COVID-19 propagation mechanism was proposed by [45] as follows:

$$\begin{cases} \dfrac{d\mathbf{S}}{d\mathbf{t}} = \Lambda + \varphi_2(1-\vartheta)\mathbf{Q} + \xi\mathbf{R} - (\psi\mathbf{I} + \chi)\mathbf{S}, \\ \dfrac{d\mathbf{E}}{d\mathbf{t}} = \psi\mathbf{IS} - (\eta_1 + \eta_2 + \chi)\mathbf{E}, \\ \dfrac{d\mathbf{Q}}{d\mathbf{t}} = \eta_2\mathbf{E} - (\chi + \varphi_2)\mathbf{Q}, \\ \dfrac{d\mathbf{I}}{d\mathbf{t}} = \eta_1\mathbf{E} - (\varphi_1 + \zeta_1 + \chi)\mathbf{I}, \\ \dfrac{d\mathbf{J}}{d\mathbf{t}} = \varphi_1\mathbf{I} + \varphi_2\vartheta\mathbf{Q} - (\chi + \zeta_2)\mathbf{J}, \\ \dfrac{d\mathbf{R}}{d\mathbf{t}} = \zeta_1\mathbf{I} + \zeta_2\mathbf{J} - (\xi + \chi)\mathbf{R}, \end{cases} \tag{1}$$

supplemented to the positive ICs $\mathbf{S} \geq 0,\ \mathbf{E} \geq 0,\ \mathbf{Q} \geq 0,\ \mathbf{I} \geq 0,\ \mathbf{J} \geq 0,\ \mathbf{R} \geq 0.$

Furthermore, current outcomes indicate that white noise can disrupt the transmission of contagious diseases, population movement, and the formulation of prevention mechanisms. As a result, an increasing number of researchers have researched the appropriate stochastic models (see [46–48]). In [49], Atangana et al. presented deterministic-stochastic modelling with crossover effects. Rashid et al. [50] proposed the novel dynamics of a stochastic fractal-fractional immune effector response to viral infection via latently infectious tissues. Regarding the epidemiologist's ideas, we assume that randomized white noise is independent and directly proportional to six cohorts. The stochastic form pertaining to scheme (1) can therefore be represented by the stochastic differential equations shown below:

$$\begin{cases} d\mathbf{S}(\mathbf{t}) = \big(\Lambda + \varphi_2(1-\vartheta)\mathbf{Q} + \xi\mathbf{R} - (\psi\mathbf{I} + \chi)\mathbf{S}\big) + \wp_1\mathbf{S}(\mathbf{t})d\mathscr{W}_1(\mathbf{t}), \\ d\mathbf{E}(\mathbf{t}) = \big(\psi\mathbf{IS} - (\eta_1 + \eta_2 + \chi)\mathbf{E}\big) + \wp_2\mathbf{E}(\mathbf{t})d\mathscr{W}_2(\mathbf{t}), \\ d\mathbf{Q}(\mathbf{t}) = \big(\eta_2\mathbf{E} - (\chi + \varphi_2)\mathbf{Q}\big) + \wp_3\mathbf{Q}(\mathbf{t})d\mathscr{W}_3(\mathbf{t}), \\ d\mathbf{I}(\mathbf{t}) = \big(\eta_1\mathbf{E} - (\varphi_1 + \zeta_1 + \chi)\mathbf{I}\big) + \wp_4\mathbf{I}(\mathbf{t})d\mathscr{W}_4(\mathbf{t}), \\ d\mathbf{J}(\mathbf{t}) = \big(\varphi_1\mathbf{I} + \varphi_2\vartheta\mathbf{Q} - (\chi + \zeta_2)\mathbf{J}\big) + \wp_5\mathbf{J}(\mathbf{t})d\mathscr{W}_5(\mathbf{t}), \\ d\mathbf{R}(\mathbf{t}) = \big(\zeta_1\mathbf{I} + \zeta_2\mathbf{J} - (\xi + \chi)\mathbf{R}\big) + \wp_6\mathbf{R}(\mathbf{t})d\mathscr{W}_6(\mathbf{t}), \end{cases} \tag{2}$$

where $\mathscr{W}_\iota$, $\iota = 1, \ldots, 6$ are two independent standard Brownian motions described on a complete filtered probability space $(\Theta, \mathscr{F}, \{\mathscr{F}_\xi\}_{\xi\geq 0}, \mathbf{P})$ involving a $\wp$-filtration $\{\mathscr{F}_\xi\}_{\xi\geq 0}$ [51]. $\wp_\iota \geq 0$, $\iota = 1, \ldots, 6$ represents the intensities of the system. Here, we provide the accompanying description to help readers who are acquainted with fractional calculus (see [34,39,40]).

$${}_0^C\mathbf{D}_\mathbf{t}^\beta \mathscr{F}(\mathbf{t}) = \frac{1}{\Gamma(1-\beta)} \int_0^\mathbf{t} \mathscr{F}'(\mathbf{r})(\mathbf{t}-\mathbf{r})^\beta d\mathbf{r}, \quad \beta \in (0, 1]. \tag{3}$$

$${}_0^{CF}\mathbf{D}_\mathbf{t}^\beta \mathscr{F}(\mathbf{t}) = \frac{\mathscr{M}(\beta)}{1-\beta} \int_0^\mathbf{t} \mathscr{F}'(\mathbf{r}) \exp\left[-\frac{\beta}{1-\beta}(\mathbf{t}-\mathbf{r})\right] d\mathbf{r}, \quad \beta \in (0, 1], \tag{4}$$

where $\mathscr{M}(\beta)$ is defined to be normalized function having $\mathscr{M}(0) = \mathscr{M}(1) = 1$.

The formulation of the Atangana-Baleanu derivative is represented below:

$${}_0^{ABC}\mathbf{D}_\mathbf{t}^\beta \mathscr{F}(\mathbf{t}) = \frac{ABC(\beta)}{1-\beta} \int_0^\mathbf{t} \mathscr{F}'(\mathbf{r}) E_\beta\left[-\frac{\beta}{1-\beta}(\mathbf{t}-\mathbf{r})^\beta\right] d\mathbf{r}, \quad \beta \in (0, 1], \tag{5}$$

where $ABC(\beta) = 1 - \beta + \dfrac{\beta}{\Gamma(\beta)}$ signifies the normalization function.

3 Qualitative Aspects of COVID-19 Model

In this section, we will discuss some qualitative aspects of the deterministic and stochastic characteristics of the COVID-19 models (1) and (2), respectively.

3.1 Deterministic Case

For COVID-19 model (1), there are two kind of steady states. The first one is disease-free equilibrium point (DFEP) $\mathscr{E}_0 = \left(\dfrac{\Lambda}{\chi}, 0, 0, 0, 0, 0\right)$ which always exists. According to [45], $\mathbb{R}_0$ is the basic reproduction number

$$\mathbb{R}_0 = \frac{\Lambda\psi\eta_1}{\chi(\eta_1 + \eta_2 + \chi)(\varphi_1 + \zeta_1 + \chi)}.$$

Notice that if $\mathbb{R}_0 > 1$, in addition to the DFEP, model (1) has a fixed non-negative endemic equilibrium point (EEP) $\mathscr{E}^* = (\mathbf{S}^*, \mathbf{E}^*, \mathbf{Q}^*, \mathbf{I}^*, \mathbf{J}^*, \mathbf{R}^*)$, where

$$\mathscr{E}^* = \Bigg(\frac{(\eta_1+\eta_2+\chi)(\varphi_1+\zeta_1+\chi)}{\psi\eta_1}, \frac{\varphi_1+\zeta_1+\chi}{\eta_1}, \frac{\eta_2(\varphi_1+\zeta_1+\chi)}{\eta_1(\varphi_2+\chi)}\mathbf{I}^*,$$
$$\frac{\chi(\eta_1+\eta_2+\chi)(\varphi_1+\zeta_1+\chi)-\psi\eta_1\Lambda}{\psi\eta_1(\varphi_2(1-\vartheta)\Psi_1+\xi\Psi_2)-\psi(\eta_1+\eta_2+\chi)(\varphi_1+\zeta_1+\chi)}, \frac{\varphi_1\eta_1(\varphi_2+\chi)+\varphi_2\vartheta\eta_2(\varphi_1+\zeta_1+\chi)}{\eta_1(\varphi_2+\chi)(\zeta_2+\chi)}\mathbf{I}^*,$$
$$\frac{\eta_1(\varphi_2+\chi)(\zeta_1(\zeta_2+\chi)+\varphi_1)+\varphi_2\vartheta\eta_2(\varphi_1+\zeta_1+\chi)}{\eta_1(\varphi_2+\chi)(\zeta_2+\chi)}\mathbf{I}^*\Bigg), \tag{6}$$

where $\Psi_1 = \dfrac{\eta_2(\varphi_1+\zeta_1+\chi)}{\beta_1(\chi+\varphi_2)}$ and $\Psi_2 = \dfrac{1}{\xi+\chi}\left(\zeta_1 + \dfrac{\zeta_2(\varphi_1+\varphi_2\vartheta\Psi_1)}{\chi+\zeta_2}\right)$.

Theorem 3.1. (i) If $\mathbb{R}_0 < 1$, the DFEP $\mathscr{E}_0$ is locally asymptotically stable.

(ii) If $\mathbb{R}_0 > 1$, the DFEP $\mathscr{E}_0$ is unstable but *EEP* $\mathscr{E}^*$ is locally asymptotically stable.

Proof. The proof can be followed by [45].

3.2 Strength Number

In previous decades, the idea of reproduction has been extensively used in epidemiological modelling since it has been recognized as a valuable mathematical tool for evaluating reproduction in a specific illness. According to the concept proposed by Atangana [52], one will identify two components $\mathbf{F}$ and $\tilde{\mathbf{V}}$, then

$$(\mathbf{F}\tilde{\mathbf{V}} - \lambda\mathbf{I}) = 0$$

will be analyzed to generate reproductive number [53]. The component $\mathbf{F}$ is particularly intriguing because it is derived from the nonlinear part of the infected classes.

$$\frac{\partial}{\partial\mathbf{I}}\left(\frac{\mathbf{I}}{\mathbf{N}}\right) = \frac{[\mathbf{N}-\mathbf{I}]}{\mathbf{N}^2}$$

and

$$\frac{\partial^2}{\partial\mathbf{I}^2}\left(\frac{(\mathbf{N}-\mathbf{I})}{\mathbf{N}^2}\right) = -2\frac{[\mathbf{N}-\mathbf{I}]}{\mathbf{N}^3}$$
$$= \frac{-2(\mathbf{S}+\mathbf{E}+\mathbf{Q}+\mathbf{J}+\mathbf{R})}{(\mathbf{S}+\mathbf{E}+\mathbf{Q}+\mathbf{I}+\mathbf{J}+\mathbf{R})^3}.$$

At disease free equilibrium $\mathscr{E}_0 = \left(\dfrac{\Lambda}{\chi}, 0, 0, 0, 0, 0\right)$, we have

$$\frac{\partial^2}{\partial\mathbf{I}^2}\left(\frac{(\mathbf{N}-\mathbf{I})}{\mathbf{N}^2}\right) = \frac{-2(\mathbf{S}_0)}{(\mathbf{S}_0)^3}.$$

Therefore, we have

$$\mathbf{F}_{\mathscr{A}} = \begin{bmatrix} 0 & 0 & \dfrac{-2(\eta_1 \mathbf{S}_0)}{(\mathbf{S}_0)^3} & 0 \\ 0 & 0 & 0 & 0 \\ 0 & 0 & 0 & 0 \end{bmatrix} = \begin{bmatrix} 0 & 0 & \dfrac{-2\eta_1 \chi^2}{\Lambda^2} & 0 \\ 0 & 0 & 0 & 0 \\ 0 & 0 & 0 & 0 \end{bmatrix}.$$

Then,

$$\det(\mathbf{F}_{\mathscr{A}} \mathbf{V}^{-1} - \lambda \mathbf{I}) = 0$$

gives

$$\mathscr{A} = \frac{-2\eta_1 \psi \Lambda}{\chi(\eta_1 + \eta_2 + \chi)(\varphi_1 + \zeta_1 + \chi)} < 0.$$

Also, $\mathscr{A}$ indicates that the expansion will not repeat and will consequently have a single magnitude and wipe out. $\mathscr{A} > 0$ indicates that there is sufficient intensity to initiate the regeneration phase, implying that the dispersion will have more than one cycle. Consequently, researchers will supply a strong insight of the aforesaid number.

3.3 Dynamic of the Stochastic COVID-19 Model

In this paper, suppose a complete probability space $(\Theta, \mathscr{F}, \{\mathscr{F}_{\mathbf{t}}\}_{\mathbf{t}\geq 0}, \mathbf{P})$ fulfilling the given assumptions (That is., it is nondecreasing and right continuous whilst $\mathscr{F}_0$ have all empty sets $\mathbf{P}$), indicating $\mathbf{R}_+ = [0,\infty)$, $\mathbf{R}_+^d = \{\mathbf{x} = (\mathbf{x}_1, \ldots, \mathbf{x}_d) \mid \mathbf{x}_i > 0, \quad i \in [1,d]\}$. Also, there is an integral mapping $\mathscr{F}_1(\mathbf{t})$ defined on $[0,\infty)$. Introducing $\mathscr{F}_1^u = \sup\{\mathscr{F}_1(\mathbf{t}) \mid \mathbf{t} \geq 0\}$, $\mathscr{F}_1^l = \inf\{\mathscr{F}_1(\mathbf{t}) \mid \mathbf{t} \geq 0\}$.

Next, we will examine at the d-dimensional stochastic DE

$$d\mathbf{Y}(\mathbf{t}) = \mathscr{F}_1(\mathbf{Y}(\mathbf{t}),\mathbf{t})d\mathbf{t} + \mathscr{G}(\mathbf{Y}(\mathbf{t}),\mathbf{t})dB(\mathbf{t}), \quad t \geq t_0$$

subject to intial condition $\mathbf{Y}(0) = X_0 \in \mathbf{R}^d$, $B(\mathbf{t})$ denotes a d-dimensional standard Brownian motion presented on the complete probability space $(\Theta, \mathscr{F}, \{\mathscr{F}_{\mathbf{t}}\}_{\mathbf{t}\geq 0}, \mathbf{P})$. Suppose $\mathbb{C}^{2,1}(\mathbf{R}^d \times [t_0,\infty]; \mathbf{R}_+)$ the collection of all positive $\mathscr{H}(\mathbf{x},\mathbf{t})$ on $\mathbf{R}^d \times [t_0,\infty]$ such that continuous twice differentiable in $\mathbf{Y}$ and once in $\mathbf{t}$. The differential operator $\mathbb{L}$ is proposed by [54]:

$$\mathbb{L} = \frac{\partial}{\partial \mathbf{t}} + \sum_{\iota=1}^{d_1} f_\iota(\mathbf{Y},\mathbf{t}) \frac{\partial}{\partial X_\iota} + \frac{1}{2} \sum_{\iota,\kappa=1}^{d_1} \left[\mathscr{G}^{\mathbf{T}}(\mathbf{Y},\mathbf{t})\mathscr{G}(\mathbf{Y},\mathbf{t})\right]_{\iota\kappa} \frac{\partial^2}{\partial X_\iota \partial X_\kappa}.$$

Now $\mathbb{L}$ imposed on a mapping $\mathscr{H} \in \mathbb{C}^{2,1}(\mathbf{R}^d \times [t_0,\infty]; \mathbf{R}_+)$, we have

$$\mathbb{L}\mathscr{H}(\mathbf{Y},\mathbf{t}) = \mathscr{H}_{\mathbf{t}}(\mathbf{Y},\mathbf{t}) + \mathscr{H}_{\mathbf{x}}(\mathbf{Y},\mathbf{t})\mathscr{F}_1(\mathbf{Y},\mathbf{t}) + \frac{1}{2} trac\left[\mathscr{G}^{\mathbf{T}}(\mathbf{Y},\mathbf{t})\mathscr{H}_{\mathbf{xx}}\mathscr{G}(\mathbf{Y},\mathbf{t})\right],$$

where $\mathscr{H}_{\mathbf{t}} = \dfrac{\partial \mathscr{H}}{\partial \mathbf{t}}, \mathscr{H}_{\mathbf{x}} = \left(\dfrac{\partial \mathscr{H}}{\partial \mathbf{x}_1}, \ldots, \dfrac{\partial \mathscr{H}}{\partial \mathbf{x}_d}\right), \quad \mathscr{H}_{\mathbf{xx}} = \left(\dfrac{\partial^2 \mathscr{H}}{\partial \mathbf{x}_\iota \partial \mathbf{x}_\kappa}\right)_{d_1 \times d_1}$. By the Itô's technique, if $\mathbf{Y}(\mathbf{t}) \in \mathbf{R}^{d_1}$, then

$$d\mathscr{H}(\mathbf{Y}(\mathbf{t}),\mathbf{t}) = \mathbb{L}\mathscr{H}(\mathbf{Y}(\mathbf{t}),\mathbf{t})d\mathbf{t} + \mathscr{H}_{\mathbf{x}}(\mathbf{Y}(\mathbf{t}),\mathbf{t})\mathscr{G}(\mathbf{Y}(\mathbf{t}),\mathbf{t})dB(\mathbf{t}).$$

3.4 Existence-Uniqueness of the Global Non-Negative Solution

Theorem 3.2. Suppose there is a unique solution $(\mathbf{S}(\mathbf{t}), \mathbf{E}(\mathbf{t}), \mathbf{Q}(\mathbf{t}), \mathbf{I}(\mathbf{t}), \mathbf{J}(\mathbf{t}), \mathbf{R}(\mathbf{t}))$ of model (2) on $\mathbf{t} \geq 0$ for every initial data $(\mathbf{S}(\mathbf{t}), \mathbf{E}(\mathbf{t}), \mathbf{Q}(\mathbf{t}), \mathbf{I}(\mathbf{t}), \mathbf{J}(\mathbf{t}), \mathbf{R}(\mathbf{t})) \in \mathbb{R}^6_+$ and the unique solution of stochastic model (2) will stay in $\mathbb{R}^6_+$ having probability 1.

Proof. Our argument is predicated on the research of Mao et al. [55]. Because the parameters of scheme (2) are Lipschitz continuous locally. As a result, there is a unique local solution $(\mathbf{S}, \mathbf{E}, \mathbf{Q}, \mathbf{I}, \mathbf{J}, \mathbf{R})$ on $\mathbf{t} \in (0, \rho_0)$ for every ICs $(\mathbf{S}(0), \mathbf{E}(0), \mathbf{Q}(0), \mathbf{I}(0), \mathbf{J}(0), \mathbf{R}(0)) \in \mathbf{R}^6_+$, where ρ_0, where ρ_0 is the moment of the explosive. We simply require to demonstrate $\rho_0 = \infty$ (a.s) to show the local solution is global. Allow ℓ_0 to be large enough for each factor of $(\mathbf{S}(0), \mathbf{E}(0), \mathbf{Q}(0), \mathbf{I}(0), \mathbf{J}(0), \mathbf{R}(0))$ inside this interval $\left[1/\ell_0, \ell_0\right]$ for every integer $\ell \geq \ell_0$, now introducing the stopping time

$$
\begin{aligned}
\rho_\ell = \inf &\left\{\mathbf{t} \in [0, \rho_0] \mid \min\{\mathbf{S}(\mathbf{t}), \mathbf{E}(\mathbf{t}), \mathbf{Q}(\mathbf{t}), \mathbf{I}(\mathbf{t}), \mathbf{J}(\mathbf{t}), \mathbf{R}(\mathbf{t})\right\} \leq \frac{1}{\ell} \\
&\quad \textit{or} \quad \max\{\mathbf{S}(\mathbf{t}), \mathbf{E}(\mathbf{t}), \mathbf{Q}(\mathbf{t}), \mathbf{I}(\mathbf{t}), \mathbf{J}(\mathbf{t}), \mathbf{R}(\mathbf{t})\} \geq \ell\Big\}.
\end{aligned}
$$

Setting $\inf\{\emptyset\} = \infty$. Note that when $\ell \mapsto \infty$ then ρ_ℓ is nondecreasing. Taking $\rho_\infty = \lim_{\ell \mapsto \infty} \rho_\ell$, therefore $\rho_\infty \leq \rho_0 \quad (a.s)$. We intend to prove $\rho_\infty = \infty \quad (a.s)$ then $\rho_0 = \infty \quad (a.s)$, which implies that $(\mathbf{S}, \mathbf{E}, \mathbf{Q}, \mathbf{I}, \mathbf{J}, \mathbf{R}) \in \mathbf{R}^6_+, \quad \forall \mathbf{t} \geq 0$. Also, if $\rho_\infty \quad (a.s)$, then there are two constants $\mathbf{T} \geq 0$ and $\varepsilon \in (0, 1)$ such that $\mathbf{P}\{\rho_\infty \leq \mathbf{T}\} \geq \epsilon$. Therefore, there is an integer $\ell_1 \geq \ell_0$ such that

$$
\mathbf{P}\{\rho_\ell \leq \mathbf{T}\} \geq \epsilon, \quad \forall \ell \geq \ell_1. \tag{7}
$$

Introducing a $\mathbb{C}^2$-functional $\hat{V} : \mathbb{R}^6_+ \mapsto \mathbb{R}_+$, i.e.,

$$
\hat{V}(\mathbf{S}, \mathbf{E}, \mathbf{Q}, \mathbf{I}, \mathbf{J}, \mathbf{R}) = (\mathbf{S} + \mathbf{E} + \mathbf{Q} + \mathbf{I} + \mathbf{J} + \mathbf{R}) - 7 - \ln(\mathbf{S} + \mathbf{E} + \mathbf{Q} + \mathbf{I} + \mathbf{J} + \mathbf{R}).
$$

The positivity of the $\mathbb{C}^2$-function $\hat{V}$ can be observed from $u_1 - 1 - \ln u_1 \geq 0, \quad \forall u_1 > 0$.

implementing Ito's rule, we can obtain that

$$
\begin{aligned}
d\hat{V}(\mathbf{S}, \mathbf{E}, \mathbf{Q}, \mathbf{I}, \mathbf{J}, \mathbf{R}) = \mathbb{L}\hat{V}(\mathbf{S}, \mathbf{E}, \mathbf{Q}, \mathbf{I}, \mathbf{J}, \mathbf{R})d\mathbf{t} &+ \wp_1(\mathbf{S} - 1)d\mathscr{W}_1(\mathbf{t}) + \wp_2(\mathbf{E} - 1)d\mathscr{W}_2(\mathbf{t}) \\
&+ \wp_3(\mathbf{Q} - 1)d\mathscr{W}_3(\mathbf{t}) + \wp_4(\mathbf{I} - 1)d\mathscr{W}_4(\mathbf{t}) + \wp_5(\mathbf{J} - 1)d\mathscr{W}_5(\mathbf{t}) \\
&+ \wp_6(\mathbf{R} - 1)d\mathscr{W}_6(\mathbf{t}),
\end{aligned}
$$

where

$$
\begin{aligned}
d\hat{V}(\mathbf{S}, \mathbf{E}, \mathbf{Q}, \mathbf{I}, \mathbf{J}, \mathbf{R}) = &\left(1 - \frac{1}{\mathbf{S}}\right)\left\{\Lambda + \varphi_2(1 - \vartheta)\mathbf{Q} + \xi\mathbf{R} - (\psi\mathbf{I} + \chi)\mathbf{S}\right\} + \frac{\wp_1^2}{2} \\
&+ \left(1 - \frac{1}{\mathbf{E}}\right)\left\{\psi\mathbf{I}\mathbf{S} - (\eta_1 + \eta_2 + \chi)\mathbf{E}\right\} + \frac{\wp_2^2}{2} \\
&+ \left(1 - \frac{1}{\mathbf{Q}}\right)\left\{\eta_2\mathbf{E} - (\chi + \varphi_2)\mathbf{Q}\right\} + \frac{\wp_3^2}{2} \\
&+ \left(1 - \frac{1}{\mathbf{I}}\right)\left\{\eta_1\mathbf{E} - (\varphi_1 + \zeta_1 + \chi)\mathbf{I}\right\} + \frac{\wp_4^2}{2}
\end{aligned}
$$

$$
\begin{aligned}
&+\left(1-\frac{1}{\mathbf{J}}\right)\left\{\varphi_1\mathbf{I}+\varphi_2\vartheta\mathbf{Q}-(\chi+\zeta_2)\mathbf{J}\right\}+\frac{\wp_5^2}{2}\\
&+\left(1-\frac{1}{\mathbf{R}}\right)\left\{\zeta_1\mathbf{I}+\zeta_2\mathbf{J}-(\xi+\chi)\mathbf{R}\right\}+\frac{\wp_6^2}{2}\\
\le{}& \Lambda+4\chi+\eta_1+\eta_2+\varphi_1+\varphi_2+\zeta_1+\zeta_2-\xi-\frac{\Lambda}{\mathbf{S}}-\varphi_2(1-\vartheta)\frac{\mathbf{Q}}{\mathbf{S}}-\xi\frac{\mathbf{R}}{\mathbf{S}}-\psi\frac{\mathbf{IS}}{\mathbf{E}}\\
&-\eta_2\frac{\mathbf{E}}{\mathbf{Q}}-\eta_1\frac{\mathbf{E}}{\mathbf{I}}-\varphi_1\frac{\mathbf{I}}{\mathbf{J}}-\varphi_2\vartheta\frac{\mathbf{Q}}{\mathbf{J}}+\zeta_1\frac{\mathbf{I}}{\mathbf{R}}-\zeta_2\frac{\mathbf{J}}{\mathbf{R}}-\chi(\mathbf{S}+\mathbf{E}+\mathbf{Q}+\mathbf{I}+\mathbf{J}+\mathbf{R})\\
&+\frac{1}{2}\left(\wp_1^2+\wp_2^2+\wp_3^2+\wp_4^2+\wp_5^2+\wp_6^2\right)\\
\le{}& \Lambda+4\chi+\eta_1+\eta_2+\varphi_1+\varphi_2+\zeta_1+\zeta_2-\xi\\
&+\frac{1}{2}\left(\wp_1^2+\wp_2^2+\wp_3^2+\wp_4^2+\wp_5^2+\wp_6^2\right):=\Upsilon_1.
\end{aligned}
$$

Therefore, we derive

$$
\begin{aligned}
d\hat{V}(\mathbf{S},\mathbf{E},\mathbf{Q},\mathbf{I},\mathbf{J},\mathbf{R})\le{}& \Upsilon_1 d\mathbf{t}+\wp_1(\mathbf{S}-1)d\mathscr{W}_1(\mathbf{t})+\wp_2(\mathbf{E}-1)d\mathscr{W}_2(\mathbf{t})\\
&+\wp_3(\mathbf{Q}-1)d\mathscr{W}_3(\mathbf{t})+\wp_4(\mathbf{I}-1)d\mathscr{W}_4(\mathbf{t})+\wp_5(\mathbf{J}-1)d\mathscr{W}_5(\mathbf{t})\\
&+\wp_6(\mathbf{R}-1)d\mathscr{W}_6(\mathbf{t}),
\end{aligned}
$$

Furthermore, we have

$$
\begin{aligned}
&\int_0^{\rho_\ell\wedge\mathbf{T}} d\hat{V}(\mathbf{S}(\mathbf{t}),\mathbf{E}(\mathbf{t}),\mathbf{Q}(\mathbf{t}),\mathbf{I}(\mathbf{t}),\mathbf{J}(\mathbf{t}),\mathbf{R}(\mathbf{t}))\\
&\le \int_0^{\rho_\ell\wedge\mathbf{T}}\Upsilon_1 d\mathbf{t}+\int_0^{\rho_\ell\wedge\mathbf{T}}\wp_1(\mathbf{S}-1)d\mathscr{W}_1(\mathbf{t})d\mathbf{t}+\int_0^{\rho_\ell\wedge\mathbf{T}}\wp_2(\mathbf{E}-1)d\mathscr{W}_2(\mathbf{t})d\mathbf{t}\\
&\quad+\int_0^{\rho_\ell\wedge\mathbf{T}}\wp_3(\mathbf{Q}-1)d\mathscr{W}_3(\mathbf{t})d\mathbf{t}+\int_0^{\rho_\ell\wedge\mathbf{T}}\wp_4(\mathbf{I}-1)d\mathscr{W}_4(\mathbf{t})d\mathbf{t}+\int_0^{\rho_\ell\wedge\mathbf{T}}\wp_5(\mathbf{J}-1)d\mathscr{W}_5(\mathbf{t})d\mathbf{t}\\
&\quad+\int_0^{\rho_\ell\wedge\mathbf{T}}\wp_6(\mathbf{R}-1)d\mathscr{W}_6(\mathbf{t})d\mathbf{t}.
\end{aligned}
$$

Implementing expectation gives

$$
\begin{aligned}
&\mathbb{E}\hat{V}(\mathbf{S}(\rho_\ell\wedge\mathbf{T}),\mathbf{E}(\rho_\ell\wedge\mathbf{T}),\mathbf{Q}(\rho_\ell\wedge\mathbf{T}),\mathbf{I}(\rho_\ell\wedge\mathbf{T}),\mathbf{J}(\rho_\ell\wedge\mathbf{T}),\mathbf{R}(\rho_\ell\wedge\mathbf{T}))\\
&\le \Upsilon_1\mathbb{E}(\rho_\ell\wedge\mathbf{T})+\hat{V}(\mathbf{S}(0),\mathbf{E}(0),\mathbf{Q}(0),\mathbf{I}(0),\mathbf{J}(0),\mathbf{R}(0))\\
&\le \Upsilon_1\mathbf{T}+\hat{V}(\mathbf{S}(0),\mathbf{E}(0),\mathbf{Q}(0),\mathbf{I}(0),\mathbf{J}(0),\mathbf{R}(0)).
\end{aligned}
$$

For $\ell\ge\ell_1$, suppose $\Theta_\ell=\{\rho_\ell\le\mathbf{T}\}$, from (7), then $\mathbf{P}(\Theta_\ell)\ge\epsilon$. Obviously, for each $\nu\in\Theta_\ell$, there is one or more of $\mathbf{S}(\rho_\ell,\nu),\mathbf{E}(\rho_\ell,\nu),\mathbf{Q}(\rho_\ell,\nu),\mathbf{I}(\rho_\ell,\nu),\mathbf{J}(\rho_\ell,\nu)$ and $\mathbf{R}(\rho_\ell,\nu)$ equals either

$1/\ell$ or ℓ, therefore $\hat{V}\big(\mathbf{S}(\rho_\ell,\nu),\mathbf{E}(\rho_\ell,\nu),\mathbf{Q}(\rho_\ell,\nu),\mathbf{I}(\rho_\ell,\nu),\mathbf{J}(\rho_\ell,\nu),\mathbf{R}(\rho_\ell,\nu)\big)$ is not less than either $\ell - 1\ln\ell$ or $1/\ell - 1 + \ln\ell$, then

$$\begin{aligned}
&\Upsilon_1\mathbf{T} + \hat{V}(\mathbf{S}(0),\mathbf{E}(0),\mathbf{Q}(0),\mathbf{I}(0),\mathbf{J}(0),\mathbf{R}(0))\\
&\geq \mathbb{E}\big[\mathscr{I}_{\Theta_\ell}(\nu)\hat{V}(\mathbf{S}(\rho_\ell,\nu),\mathbf{E}(\rho_\ell,\nu),\mathbf{Q}(\rho_\ell,\nu),\mathbf{I}(\rho_\ell,\nu),\mathbf{J}(\rho_\ell,\nu),\mathbf{R}(\rho_\ell,\nu))\big]\\
&\geq \epsilon(\ell - 1 - \ln\ell)\wedge\big(1/\ell - 1 + \ln\ell\big),
\end{aligned}$$

where $\mathscr{I}_{\Theta_\ell}(.)$ represents the indicating mapping of Θ_ℓ. Thus, applying limit $\ell \mapsto \infty$ yields contradiction

$$\infty = \Upsilon_1\mathbf{T} + \hat{V}(\mathbf{S}(0),\mathbf{E}(0),\mathbf{Q}(0),\mathbf{I}(0),\mathbf{J}(0),\mathbf{R}(0)) < \infty.$$

Thus, we find $\rho_\infty = \infty$, $(a.s)$. This completes the proof.

3.5 Basic Reproduction Number for Stochastic Model

Utilizing fourth compartment of the model (2), we have

$$d\mathbf{I}(\mathbf{t}) = \big(\eta_1\mathbf{E} - (\varphi_1 + \zeta_1 + \chi)\mathbf{I}\big) + \wp_4\mathbf{I}(\mathbf{t})d\mathscr{W}_4(\mathbf{t}).$$

Considering Ito's formulation for a twice differentiable mapping $\mathscr{F}(\mathbf{I}) = \ln(\mathbf{I})$, and expanding by Taylor series

$$\begin{aligned}
d\mathscr{F}(\mathbf{t},\mathbf{I}(\mathbf{t})) &= \frac{\partial\mathscr{F}}{\partial\mathbf{t}}d\mathbf{t} + \frac{\partial\mathscr{F}}{\partial\mathbf{I}}d\mathbf{I} + \frac{1}{2}\frac{\partial^2\mathscr{F}}{\partial\mathbf{I}^2}(d\mathbf{I})^2 + \frac{\partial^2\mathscr{F}}{\partial\mathbf{t}\partial\mathbf{I}}d\mathbf{I}d\mathbf{t} + \frac{1}{2}\frac{\partial^2\mathscr{F}}{\partial\mathbf{t}^2}(d\mathbf{t})^2,\\
&\Longrightarrow d\mathscr{F}(\mathbf{t},\mathbf{I}(\mathbf{t})) = 0.d\mathbf{t} + \frac{1}{\mathbf{I}}\Big\{(\eta_1\mathbf{E} - (\varphi_1 + \zeta_1 + \chi)\mathbf{I})d\mathbf{t} + \wp_4\mathbf{I}d\mathscr{W}_4(\mathbf{t})\Big\}\\
&\quad - \frac{1}{2\mathbf{I}^2}\Big\{(\eta_1\mathbf{E} - (\varphi_1 + \zeta_1 + \chi)\mathbf{I})d\mathbf{t} + \wp_4\mathbf{I}d\mathscr{W}_4(\mathbf{t})\Big\}^2\\
&\Longrightarrow d\mathscr{F}(\mathbf{t},\mathbf{I}(\mathbf{t})) = \Big\{(\eta_1\mathbf{E} - (\varphi_1 + \zeta_1 + \chi))d\mathbf{t} + \wp_4 d\mathscr{W}_4(\mathbf{t})\Big\}\\
&\quad - \frac{1}{2\mathbf{I}^2}\Big\{\mathscr{Q}_1^2(d\mathbf{t})^2 + 2\mathscr{Q}_1\mathscr{Q}_2 d\mathbf{t}d\mathscr{W}_4(\mathbf{t}) + \mathscr{Q}_2^2(d\mathscr{W}_4(\mathbf{t}))^2\Big\},
\end{aligned}$$

where $\mathscr{Q}_1 = \eta_1\mathbf{E} - (\varphi_1 + \zeta_1 + \chi)\mathbf{I}$ and $\mathscr{Q}_2 = \wp_4\mathbf{I}$,

$$\begin{aligned}
&\Longrightarrow d\mathscr{F}(\mathbf{t},\mathbf{I}(\mathbf{t})) = \Big\{(\eta_1\mathbf{E} - (\varphi_1 + \zeta_1 + \chi))d\mathbf{t} + \wp_4 d\mathscr{W}_4(\mathbf{t})\Big\} - \frac{1}{2\mathbf{I}^2}\Big\{\mathscr{Q}_2^2(d\mathscr{W}_4(\mathbf{t}))^2\Big\}\\
&\Longrightarrow d\mathscr{F}(\mathbf{t},\mathbf{I}(\mathbf{t})) = \underbrace{\Big\{(\eta_1\mathbf{E} - (\varphi_1 + \zeta_1 + \chi))d\mathbf{t} + \wp_4 d\mathscr{W}_4(\mathbf{t})\Big\} - \frac{1}{2\mathbf{I}^2}\Big\{\wp_4^2\mathbf{I}^2 d\mathbf{t}\Big\}}_{(By\ variance\ of\ Wiener\ technique)}\\
&\Longrightarrow d\mathscr{F}(\mathbf{t},\mathbf{I}(\mathbf{t})) = \Big\{(\eta_1\mathbf{E} - (\varphi_1 + \zeta_1 + \chi) - \frac{1}{2}\wp_4^2)\Big\}d\mathbf{t} + \wp_4 d\mathscr{W}_4(\mathbf{t}).
\end{aligned}$$

The next generation matrices are $\mathbf{F} = \Big[\eta_1\mathbf{E} - \frac{1}{2}\wp_4^2\Big]$ and $\mathbf{V} = \big[\varphi_1 + \zeta_1 + \chi\big]$. At DFEP and by the principal of next generation matrix, the dominant eigenvalue is the basic reproductive number. Hence $\mathbb{R}_0^S = \dfrac{\wp_4^2}{2(\varphi_1 + \zeta_1 + \chi)}$.

3.6 Extinction and Persistence of the Disease

One of the primary challenges in epidemiological data is how to control infection behaviours so that the infection becomes endangered and persists throughout time. In this part, we attempt to determine the important threshold for pathogen extermination and permanence.

Lemma 3.1. For the initial settings $(\mathbf{S}(0), \mathbf{E}(0), \mathbf{Q}(0), \mathbf{I}(0), \mathbf{J}(0), \mathbf{R}(0)) \in \mathbb{R}^6_+$, the solution of the stochastic system (2) admits

$$\lim_{\mathbf{t}\mapsto\infty} \frac{\ln \mathbf{S}(\mathbf{t})}{\mathbf{t}} \le 0, \quad \lim_{\mathbf{t}\mapsto\infty} \frac{\ln \mathbf{E}(\mathbf{t})}{\mathbf{t}} \le 0, \quad \lim_{\mathbf{t}\mapsto\infty} \frac{\ln \mathbf{Q}(\mathbf{t})}{\mathbf{t}} \le 0$$
$$\lim_{\mathbf{t}\mapsto\infty} \frac{\ln \mathbf{I}(\mathbf{t})}{\mathbf{t}} \le 0, \quad \lim_{\mathbf{t}\mapsto\infty} \frac{\ln \mathbf{J}(\mathbf{t})}{\mathbf{t}} \le 0, \quad \lim_{\mathbf{t}\mapsto\infty} \frac{\ln \mathbf{R}(\mathbf{t})}{\mathbf{t}} \le 0. \ (a.s). \tag{8}$$

then

$$\lim_{\mathbf{t}\mapsto\infty} \frac{\mathbf{S}(\mathbf{t}) + \mathbf{E}(\mathbf{t}) + \mathbf{Q}(\mathbf{t}) + \mathbf{I}(\mathbf{t}) + \mathbf{J}(\mathbf{t}) + \mathbf{R}(\mathbf{t})}{\mathbf{t}} = 0, \quad a.s. \tag{9}$$

Also, if $\chi > \frac{1}{2}(\wp_1^2 \vee \wp_2^2 \vee \wp_3^2 \vee \wp_4^2 \vee \wp_5^2 \vee \wp_6^2)$, we find

$$\lim_{\mathbf{t}\mapsto\infty} \frac{1}{\mathbf{t}} \int_0^{\mathbf{t}} \mathbf{S}(\mathbf{r}) d\mathscr{W}_1(\mathbf{r}) = 0, \ \lim_{\mathbf{t}\mapsto\infty} \frac{1}{\mathbf{t}} \int_0^{\mathbf{t}} \mathbf{E}(\mathbf{r}) d\mathscr{W}_1(\mathbf{r}) = 0, \ \lim_{\mathbf{t}\mapsto\infty} \frac{1}{\mathbf{t}} \int_0^{\mathbf{t}} \mathbf{Q}(\mathbf{r}) d\mathscr{W}_1(\mathbf{r}) = 0,$$

$$\lim_{\mathbf{t}\mapsto\infty} \frac{1}{\mathbf{t}} \int_0^{\mathbf{t}} \mathbf{I}(\mathbf{r}) d\mathscr{W}_1(\mathbf{r}) = 0, \ \lim_{\mathbf{t}\mapsto\infty} \frac{1}{\mathbf{t}} \int_0^{\mathbf{t}} \mathbf{J}(\mathbf{r}) d\mathscr{W}_1(\mathbf{r}) = 0, \ \lim_{\mathbf{t}\mapsto\infty} \frac{1}{\mathbf{t}} \int_0^{\mathbf{t}} \mathbf{R}(\mathbf{r}) d\mathscr{W}_1(\mathbf{r}) = 0. \tag{10}$$

Theorem 3.3. Suppose that $\chi > \frac{1}{2}(\wp_1^2 \vee \wp_2^2 \vee \wp_3^2 \vee \wp_4^2 \vee \wp_5^2 \vee \wp_6^2)$ and assume that there is a positive solution of the system $\big(\mathbf{S}(\mathbf{t}), \mathbf{E}(\mathbf{t}), \mathbf{Q}(\mathbf{t}), \mathbf{I}(\mathbf{t}), \mathbf{J}(\mathbf{t}), \mathbf{R}(\mathbf{t})\big)$ having initial settings $(\mathbf{S}(0), \mathbf{E}(0), \mathbf{Q}(0), \mathbf{I}(0), \mathbf{J}(0), \mathbf{R}(0))$, we find

(i) If $\mathbb{R}_0^S < 1$, then

$$\limsup_{\mathbf{t}\mapsto\infty} \frac{\ln \mathbf{I}(\mathbf{t})}{\mathbf{t}} \le \left(\varphi_1 + \zeta_1 + \chi + \frac{1}{2}\wp_4^2\right)(\mathbb{R}_0^S - 1) < 0, \quad (a.s). \tag{11}$$

which means the diseases will be eliminated from a community.

(ii) If $\mathbb{R}_0^S > 1$, then

$$\liminf_{\mathbf{t}\mapsto\infty} \frac{1}{\mathbf{t}} \int_0^{\mathbf{t}} \mathbf{I}(\mathbf{r}) d\mathbf{r} \ge \frac{\left(\varphi_1 + \zeta_1 + \chi + \frac{1}{2}\wp_4^2\right)(\mathbb{R}_0^S - 1)}{\mathscr{K}_2} > 0 \quad (a.s)., \tag{12}$$

which means the diseases will persist in the community.

Proof. Implementing the Ito's formula to $\ln \mathbf{I}(\mathbf{t})$, we find

$$d \ln \mathbf{I}(\mathbf{t}) = \left\{ \left(\eta_1 \frac{\mathbf{E}}{\mathbf{I}} - (\varphi_1 + \zeta_1 + \chi) - \frac{1}{2}\wp_4^2 \right) \right\} d\mathbf{t} + \wp_4 d\mathscr{W}_4(\mathbf{t}) \tag{13}$$

Integrating the aforesaid equation from 0 to $\mathbf{t}$ on both sides, then

$$\ln \mathbf{I}(\mathbf{t}) - \ln \mathbf{I}(0) = \int_0^{\mathbf{t}} \left[\eta_1 \frac{\mathbf{E}}{\mathbf{I}} - (\varphi_1 + \zeta_1 + \chi) - \frac{1}{2}\wp_4^2 \right] d\mathbf{r} + \wp_4 \int_0^{\mathbf{t}} d\mathscr{W}_4(\mathbf{r}). \tag{14}$$

By the strong law of large numbers for martingales [56], we have $\lim_{\mathbf{t}\mapsto\infty} \frac{1}{\mathbf{t}} \int_0^{\mathbf{t}} d\mathscr{W}_4(\mathbf{r}) = 0.$ $(a.s)$.

According to the superior limit and considering stochastic comparison theorem, we have

$$\begin{aligned}
\limsup_{\mathbf{t}\mapsto\infty} \frac{\ln \mathbf{I}(\mathbf{t})}{\mathbf{t}} &= \limsup_{\mathbf{t}\mapsto\infty} \frac{1}{\mathbf{t}} \int_0^{\mathbf{t}} \left[\eta_1 \frac{\mathbf{E}}{\mathbf{I}} - (\varphi_1 + \zeta_1 + \chi + \frac{1}{2}\wp_4^2) \right] d\mathbf{r} \\
&\leq (\varphi_1 + \zeta_1 + \chi + \frac{1}{2}\wp_4^2)(\mathbb{R}_0^S - 1) < 0 \\
&\implies (\mathbb{R}_0^S - 1) < 0.
\end{aligned} \tag{15}$$

Thus, $\mathbb{R}_0^S < 1$. Hence, it shows that $\lim_{\mathbf{t}\mapsto\infty} \mathbf{I}(\mathbf{t}) = 0$, $(a.s)$.

As a result, the infection will be exterminated in the community.

(ii) Introducing $\mathbb{C}^2$-mapping V_1

$$\begin{aligned}
V_1(\mathbf{S}, \mathbf{E}, \mathbf{Q}, \mathbf{I}, \mathbf{J}, \mathbf{R}) = {} & \eta_1(\mathbf{N} - (\mathbf{S} + \mathbf{Q} + \mathbf{I} + \mathbf{J} + \mathbf{R})) + (\varphi_1 + \zeta_1 + \chi)(\mathbf{N} - (\mathbf{S} + \mathbf{Q} + \mathbf{E} + \mathbf{J} + \mathbf{R})) \\
& - \frac{1}{2}\wp_4^2 - (\varphi_1 + \zeta_1 + \chi).
\end{aligned} \tag{16}$$

Utilizing the fact of $\mathbb{R}_0^S > 1$, we have

$$\begin{aligned}
\mathbb{L}V_1((\mathbf{S}, \mathbf{E}, \mathbf{Q}, \mathbf{I}, \mathbf{J}, \mathbf{R}) = {} & \eta_1(\mathbf{N} - (\mathbf{S} + \mathbf{Q} + \mathbf{J} + \mathbf{R})) + (\varphi_1 + \zeta_1 + \chi)(\mathbf{N} - (\mathbf{S} + \mathbf{Q} + \mathbf{E} + \mathbf{J} + \mathbf{R})) \\
& - \frac{1}{2}\wp_4^2 - (\varphi_1 + \zeta_1 + \chi), \\
= {} & (\varphi_1 + \zeta_1 + \chi)\left\{ \frac{\Lambda\psi\eta_1}{\chi(\eta_1 + \eta_2 + \chi)(\varphi_1 + \zeta_1 + \chi)} - \frac{\wp_4^2}{2(\varphi_1 + \zeta_1 + \chi)} - 1 \right\} + \mathscr{K}_2\mathbf{I}.
\end{aligned} \tag{17}$$

Then,

$$dV_1(\mathbf{S}, \mathbf{E}, \mathbf{Q}, \mathbf{I}, \mathbf{J}, \mathbf{R}) \leq -(\varphi_1 + \zeta_1 + \chi)(\mathbb{R}_0^S - 1) + \mathscr{K}_2\mathbf{I}. \tag{18}$$

Assume that $\mathscr{K}_3 = \dfrac{\eta_1 + \eta_2 + \chi}{\psi\eta} + \dfrac{\eta_2}{\eta_1(\varphi_2 + \chi)}$. As a result, we have

$$\begin{aligned} dV_1(\mathbf{S},\mathbf{E},\mathbf{Q},\mathbf{I},\mathbf{J},\mathbf{R}) = \mathbb{L}V_1 d\mathbf{t} - \wp_4 d\mathscr{W}_4(\mathbf{t}) - \frac{\psi\Lambda}{\chi}\wp_1\mathbf{S}d\mathscr{W}_1(\mathbf{t}) - \frac{\eta_1+\eta_2+\chi}{\psi}\wp_2\mathbf{E}d\mathscr{W}_2(\mathbf{t}) \\ - \frac{\varphi_2+\chi}{\eta_2}\wp_3\mathbf{Q}d\mathscr{W}_3(\mathbf{t}) - \mathscr{K}_3\wp_4\mathbf{I}d\mathscr{W}_4(\mathbf{t}) - \frac{\zeta_2+\chi}{\varphi_1}\wp_5\mathbf{J}d\mathscr{W}_5(\mathbf{t}) \\ - \frac{\xi+\chi}{\zeta_1}\wp_6\mathbf{R}d\mathscr{W}_6(\mathbf{t}). \end{aligned} \tag{19}$$

Integrating both sides of (19), we find

$$\begin{aligned} &\frac{V_1(\mathbf{S}(\mathbf{t}),\mathbf{E}(\mathbf{t}),\mathbf{Q}(\mathbf{t}),\mathbf{I}(\mathbf{t}),\mathbf{J}(\mathbf{t}),\mathbf{R}(\mathbf{t})) - V_1(\mathbf{S}(0),\mathbf{E}(0),\mathbf{Q}(0),\mathbf{I}(0),\mathbf{J}(0),\mathbf{R}(0))}{\mathbf{t}} \\ &\le -(\varphi_1+\zeta_1+\chi)(\mathbb{R}_0^S - 1) + \mathscr{K}_2\frac{1}{\mathbf{t}}\int_0^{\mathbf{t}} \mathbf{I}(\mathbf{r})d\mathbf{r} - \frac{\mathscr{M}(\mathbf{t})}{\mathbf{t}} - \frac{\psi\Lambda}{\chi}\frac{1}{\mathbf{t}}\int_0^{\mathbf{t}} \wp_1\mathbf{S}\mathscr{W}_1(\mathbf{r})d\mathbf{r} \\ &\quad - \frac{\eta_1+\eta_2+\chi}{\psi}\frac{1}{\mathbf{t}}\int_0^{\mathbf{t}} \wp_2\mathbf{E}d\mathscr{W}_2(\mathbf{r}) - \frac{\varphi_2+\chi}{\eta_2}\int_0^{\mathbf{t}} \wp_3\mathbf{Q}d\mathscr{W}_3(\mathbf{r}) - \mathscr{K}_3\frac{1}{\mathbf{t}}\int_0^{\mathbf{t}} \wp_4\mathbf{I}d\mathscr{W}_4(\mathbf{r}) \\ &\quad - \frac{\zeta_2+\chi}{\varphi_1}\frac{1}{\mathbf{t}}\int_0^{\mathbf{t}} \wp_5\mathbf{J}d\mathscr{W}_5(s_1) - \frac{\xi+\chi}{\zeta_1}\frac{1}{\mathbf{t}}\int_0^{\mathbf{t}} \wp_6\mathbf{R}d\mathscr{W}_6(\mathbf{r}), \end{aligned} \tag{20}$$

where $\mathscr{M}(\mathbf{t}) = \int_0^{\mathbf{t}} \wp_4 d\mathscr{W}_4(\mathbf{r})$ represents a martingale. According to strong law of large numbers for martingales, we have $\lim\limits_{\mathbf{t}\mapsto\infty} \dfrac{M(\mathbf{t})}{\mathbf{t}} = 0, \quad (a.s)$.

Utilizing Lemma 3.1, we find from (20)

$$\begin{aligned} &\liminf_{\mathbf{t}\mapsto\infty} \mathscr{K}_2\frac{1}{\mathbf{t}}\int_0^{\mathbf{t}} \mathbf{I}(\mathbf{r})d(\mathbf{r}) \\ &\ge -(\varphi_1+\zeta_1+\chi)(\mathbb{R}_0^S - 1) \\ &\quad + \liminf_{\mathbf{t}\mapsto\infty} \frac{V_1(\mathbf{S}(\mathbf{t}),\mathbf{E}(\mathbf{t}),\mathbf{Q}(\mathbf{t}),\mathbf{I}(\mathbf{t}),\mathbf{J}(\mathbf{t}),\mathbf{R}(\mathbf{t})) - V_1(\mathbf{S}(0),\mathbf{E}(0),\mathbf{Q}(0),\mathbf{I}(0),\mathbf{J}(0),\mathbf{R}(0))}{\mathbf{t}} \\ &\ge (\varphi_1+\zeta_1+\chi)(\mathbb{R}_0^S - 1) > 0, \quad (a.s). \end{aligned}$$

Thus, if $\mathbb{R}_0^S > 1$, the sickness will remain for an extended period of time. This concludes the evidence.

3.7 Ergodic Stationary Distribution (ESD)

In this subsection, we will discuss several perspectives about the stationary distribution. Despite the fact that there is no EEP of the stochastic process (2), we wish to find the existence of an ESD, which demonstrates the virus's endurance. Several noteworthy Has'Minskii theory outcomes can be referenced in [57].

Lemma 3.2. ([58]) The Markov technique $Y_1(\mathbf{t})$ has a unique ESD $\pi(.)$ if there exists a bounded region $\mathscr{G} \subset E_1$ having regular boundary $\mathscr{D}$, and

(i) A positive number $\mathscr{M}$ such that $\sum_{\iota,\Bbbk=1}^{d} a_{\iota\Bbbk}(y_1)\xi_\iota\xi_\Bbbk \geq \mathscr{M}|\xi|^2, \quad y_1 \in \mathscr{G}, \xi \in \mathbb{R}^\iota$.

(ii) there exists a positive $\mathbb{C}^2$-function $\mathscr{V}$, such that $\mathbb{L}\mathscr{V}$ is negative for any $E_1/\mathscr{G}$. Then,

$$\mathbf{P}\left\{\lim_{\mathbf{T}\mapsto\infty}\frac{1}{\mathbf{T}}\int_0^{\mathbf{T}}\mathscr{F}(Y_1(\mathbf{t}))d\mathbf{t} = \int_{\Omega_d}\mathscr{F}(y_1)\pi(dy_1) = 1\right\},$$

for all $y_1 \in E_1$, where $\mathscr{F}(.)$ is a mapping integrable regarding to the measure $\pi(.)$.

We shall establish assumptions that assure the formation of an ESD relying on Has'minskii's hypothesis [57].

Theorem 3.4. Suppose that $\mathbb{R}_0^S > 1$, then the solution $(\mathbf{S}(\mathbf{t}), \mathbf{E}(\mathbf{t}), \mathbf{Q}(\mathbf{t}), \mathbf{I}(\mathbf{t}), \mathbf{J}(\mathbf{t}), \mathbf{R}(\mathbf{t}))$ of model (2) has a unique ESD for any initial settings $(\mathbf{S}(0), \mathbf{E}(0), \mathbf{Q}(0), \mathbf{I}(0), \mathbf{J}(0), \mathbf{R}(0)) \in \mathbb{R}_+^6$.

Proof. Theorem 3.2 proof must meet the criteria of Lemma 3.2. Ensure that **(i)** satisfies. The associated diffusion matrix of framework (2) appears to be represented by

$$\mathscr{A} = \begin{bmatrix} \wp_1^2\mathbf{S} & 0 & 0 & 0 & 0 & 0 \\ 0 & \wp_2^2\mathbf{E} & 0 & 0 & 0 & 0 \\ 0 & 0 & \wp_3^2\mathbf{Q} & 0 & 0 & 0 \\ 0 & 0 & 0 & \wp_4^2\mathbf{I} & 0 & 0 \\ 0 & 0 & 0 & 0 & \wp_5^2\mathbf{J} & 0 \\ 0 & 0 & 0 & 0 & 0 & \wp_6^2\mathbf{R} \end{bmatrix}.$$

Because the matrix $\mathscr{A}$ is clearly positive definite for any compact subset of $\mathbb{R}_+^6$, criterion **(i)** in Lemma 3.2 is achieved. Now we will demonstrate criterion **(ii)**. Construct a $\mathbb{C}^2$-function

$$\begin{aligned}\tilde{\mathscr{V}}(\mathbf{S}, \mathbf{E}, \mathbf{Q}, \mathbf{I}, \mathbf{J}, \mathbf{R}) &= \mathscr{M}(-\varpi_1\ln\mathbf{S} - \varpi_2\ln\mathbf{E} - \varpi_3\ln\mathbf{Q} - \varpi_4\ln\mathbf{I} - \varpi_6\ln\mathbf{R} - \varpi_5\mathbf{J}) \\ &\quad + \frac{1}{\vartheta+1}(\mathbf{S}+\mathbf{E}+\mathbf{Q}+\mathbf{I}+\mathbf{J}+\mathbf{R}) - \ln\mathbf{S} - \ln\mathbf{E} - \ln\mathbf{Q} - \ln\mathbf{I} - \ln\mathbf{R} \\ &:= \mathscr{M}V_1 + V_2 - \ln\mathbf{S} - \ln\mathbf{E} - \ln\mathbf{Q} - \ln\mathbf{I} - \ln\mathbf{R},\end{aligned}$$

where $\varpi_\iota, \quad \iota = 1, \ldots, 6, \quad \vartheta$ and $\mathscr{M}$ are positive constants, which can be estimated later. It is simple to verify this

$$\lim_{\kappa\mapsto\infty(\mathbf{S},\mathbf{E},\mathbf{Q},\mathbf{I},\mathbf{J},\mathbf{R})\in\mathbb{R}_+^5/\mathscr{G}_\kappa}\tilde{\mathscr{V}}(\mathbf{S}, \mathbf{E}, \mathbf{Q}, \mathbf{I}, \mathbf{J}, \mathbf{R}) = +\infty,$$

where $\mathscr{G}_\kappa = \prod_{\iota=1}^{6}\left(\frac{1}{\kappa},\kappa\right)$. Additionally, $\tilde{\mathscr{V}}(\mathbf{S},\mathbf{E},\mathbf{Q},\mathbf{I},\mathbf{J},\mathbf{R})$ is a continuous mapping. Thus, $\tilde{\mathscr{V}}(\mathbf{S},\mathbf{E},\mathbf{Q},\mathbf{I},\mathbf{J},\mathbf{R})$. There might be a minimum point $(\mathbf{S}_0,\mathbf{E}_0,\mathbf{Q}_0,\mathbf{I}_0,\mathbf{J}_0,\mathbf{R}_0)\in\mathbb{R}_+^6$. Hence, we introduce a positive $\mathbb{C}^2$-mapping $\mathscr{V}:\mathbb{R}_+^6\mapsto\mathbb{R}_+$

$$\mathscr{V}(\mathbf{S},\mathbf{E},\mathbf{Q},\mathbf{I},\mathbf{J},\mathbf{R})=\tilde{\mathscr{V}}(\mathbf{S},\mathbf{E},\mathbf{Q},\mathbf{I},\mathbf{J},\mathbf{R})-\tilde{\mathscr{V}}(\mathbf{S}_0,\mathbf{E}_0,\mathbf{Q}_0,\mathbf{I}_0,\mathbf{J}_0,\mathbf{R}_0).$$

Implementing the generalized Ito's technique [51] to $\mathscr{V}_1$, one can find the differential operator $\mathbb{L}$ of $\mathscr{V}_1$ as

$$\begin{aligned}
\mathbb{L}\mathscr{V}_1 &= -\frac{\varpi_1}{\mathbf{S}}\left\{\Lambda+\varphi_2(1-\vartheta)\mathbf{Q}+\xi\mathbf{R}-(\psi\mathbf{I}+\chi)\mathbf{S}\right\}+\frac{\varpi_1\wp_1^2}{2}-\frac{\varpi_2}{\mathbf{E}}\left(\psi\mathbf{I}\mathbf{S}-(\eta_1+\eta_2+\chi)\mathbf{E}\right)+\frac{\varpi_2\wp_2^2}{2}\\
&\quad-\frac{\varpi_3}{\mathbf{Q}}\left(\eta_2\mathbf{E}-(\chi+\varphi_2)\mathbf{Q}\right)+\frac{\varpi_3\wp_3^2}{2}-\frac{\varpi_4}{\mathbf{I}}\left(\eta_1\mathbf{E}-(\varphi_1+\zeta_1+\chi)\mathbf{I}\right)+\frac{\varpi_4\wp_4^2}{2}\\
&\quad-\varpi_5\left(\varphi_1\mathbf{I}+\varphi_2\vartheta\mathbf{Q}-(\chi+\zeta_2)\mathbf{J}\right)+\frac{\varpi_6\wp_6^2}{2}-\frac{\varpi_6}{\mathbf{R}}\left(\zeta_1\mathbf{I}+\zeta_2\mathbf{J}-(\chi+\xi)\mathbf{R}\right)\\
&\le-\left(\frac{\varpi_1(\Lambda+\varphi_2(1-\vartheta)\mathbf{Q}+\xi\mathbf{R})}{\mathbf{S}}+\frac{\varpi_2(\psi\mathbf{I}\mathbf{S})}{\mathbf{E}}+\frac{\varpi_3\eta_2\mathbf{E}}{\mathbf{Q}}+\frac{\varpi_4\eta_1\mathbf{E}}{\mathbf{I}}+\frac{\varpi_6(\zeta_1\mathbf{I}+\zeta_2\mathbf{J})}{\mathbf{R}}\right)\\
&\quad+\varpi_2(\eta_1+\eta_2+\chi)+\varpi_3(\chi+\varphi_2)+\varpi_4(\varphi_1+\zeta_1+\chi)+\varpi_5(\chi+\xi)-(\varpi_1\psi-\varphi_1\varpi_5)\mathbf{I}-(\varpi_2\chi)\\
&\quad-\varpi_5\varphi_2\vartheta\mathbf{Q}-\varpi_5(\chi+\zeta_2)\mathbf{J}+\frac{1}{2}\left(\varpi_1\wp_1^2+\varpi_2\wp_2^2+\varpi_3\wp_3^2+\varpi_4\wp_4^2+\varpi_5\wp_5^2\right)\\
&\le-5\sqrt[5]{\varpi_1\varpi_2\varpi_3\varpi_4\varpi_5(\Lambda+\varphi_2(1-\vartheta)+\xi)\psi\eta_2\eta_1(\zeta_1+\zeta_2)}+\varpi_2\left(\eta_1+\eta_2+\frac{\wp_2^2}{2}\right)\\
&\quad+\varpi_3\left(\chi+\varphi_2+\frac{\wp_3^2}{2}\right)+\varpi_4\left(\varphi_1+\zeta_1+\chi+\frac{\wp_4^2}{2}\right)+\varpi_5\left(\chi+\xi+\frac{\wp_5^2}{2}\right)-(\varpi_1\psi-\varphi_1\varpi_5)\mathbf{I}\\
&\quad-(\varpi_2\chi)-\varpi_5\varphi_2\vartheta\mathbf{Q}-\varpi_5(\chi+\zeta_2)\mathbf{J}+\frac{1}{2}\left(\varpi_1\wp_1^2\right).
\end{aligned}$$

Suppose

$$\varpi_1=1,\quad \varpi_2=\frac{\wp_1^2}{2(\eta_1+\eta_2+\wp_2^2)},\varpi_3=\frac{\wp_1^2}{2(\chi+\varphi_2+\wp_3^2)},\quad \varpi_4=\frac{\wp_1^2}{2(\varphi_1+\zeta_1+\chi+\wp_4^2)},$$
$$\varpi_5=\frac{\wp_1^2}{2(\chi+\xi+\wp_5^2)},\quad \varpi_6=\left(\frac{\mathscr{M}+1}{\mathscr{M}}\right)\frac{\psi}{\varphi_1}.$$

Then, it follows that

$$\begin{aligned}
\mathbb{L}\mathscr{V}_1 &\le -5\left[\frac{(\Lambda+\varphi_2(1-\vartheta)+\xi)\psi\eta_2\eta_1(\zeta_1+\zeta_2)\wp_1^8}{16(\eta_1+\eta_2+\wp_2^2)(\chi+\varphi_2+\wp_3^2)(\varphi_1+\zeta_1+\chi+\wp_4^2)(\chi+\xi+\wp_5^2)}\right]^{1/5}\\
&\quad-\frac{\psi}{\varphi_1}\mathbf{I}-\frac{\wp_1^2\varphi_2\vartheta}{2(\chi+\xi+\wp_5^2)}\mathbf{Q}-(\chi+\zeta_2)\frac{\wp_1^2}{2(\chi+\xi+\wp_5^2)}\\
&=-5(\wp_1^8)\left(\mathbb{R}_0^{s^{1/5}}-1\right)-\frac{\psi}{\varphi_1}\mathbf{I}-\frac{\wp_1^2\varphi_2\vartheta}{2(\chi+\xi+\wp_5^2)}\mathbf{Q}-(\chi+\zeta_2)\frac{\wp_1^2}{2(\chi+\xi+\wp_5^2)}.
\end{aligned}\tag{21}$$

Analogously, we have

$$\begin{aligned}\mathbb{L}\mathscr{V}_2 &= (\mathbf{S}+\mathbf{E}+\mathbf{Q}+\mathbf{I}+\mathbf{J}+\mathbf{R})^{\vartheta}\big[\Lambda - \vartheta(\mathbf{S}+\mathbf{E}+\mathbf{Q}+\mathbf{I}+\mathbf{J}+\mathbf{R})\big]\\ &\quad + \frac{\vartheta}{2}(\mathbf{S}+\mathbf{E}+\mathbf{Q}+\mathbf{I}+\mathbf{J}+\mathbf{R})^{\vartheta-1}(\wp_1^2\mathbf{S}^2 + \wp_2^2\mathbf{E}^2 + \wp_3^2\mathbf{Q}^2 + \wp_4^2\mathbf{I}^2 + \wp_5^2\mathbf{J}^2 + \wp_6^2\mathbf{R}^2)\\ &\leq \Lambda(\mathbf{S}+\mathbf{E}+\mathbf{Q}+\mathbf{I}+\mathbf{J}+\mathbf{R})^{\vartheta} - \vartheta(\mathbf{S}+\mathbf{E}+\mathbf{Q}+\mathbf{I}+\mathbf{J}+\mathbf{R})^{\vartheta+1}\\ &\quad + \frac{\vartheta}{2}(\wp_1^2 \vee \wp_2^2 \vee \wp_3^2 \vee \wp_4^2 \vee \wp_5^2 \vee \wp_6^2)(\mathbf{S}+\mathbf{E}+\mathbf{Q}+\mathbf{I}+\mathbf{J}+\mathbf{R})^{\vartheta+1}\\ &\leq \mathbb{C}_0 - \frac{1}{2}\rho(\mathbf{S}+\mathbf{E}+\mathbf{Q}+\mathbf{I}+\mathbf{J}+\mathbf{R})^{\vartheta+1}\\ &\leq \mathbb{C}_0 - \rho(\mathbf{S}^{\vartheta+1} + \mathbf{E}^{\vartheta+1} + \mathbf{Q}^{\vartheta+1} + \mathbf{I}^{\vartheta+1} + \mathbf{J}^{\vartheta+1} + \mathbf{R}^{\vartheta+1}),\end{aligned} \tag{22}$$

where ρ assumed to be sufficiently small such that $\rho = \wp_1^8 > 0$ and

$$\mathbb{C}_0 = \sup_{(\mathbf{S},\mathbf{E},\mathbf{Q},\mathbf{I},\mathbf{J},\mathbf{R})\in\mathbb{R}_+^6} \left\{\Lambda(\mathbf{S}+\mathbf{E}+\mathbf{Q}+\mathbf{I}+\mathbf{J}+\mathbf{R})^{\vartheta} - \frac{\rho}{2}(\mathbf{S}+\mathbf{E}+\mathbf{Q}+\mathbf{I}+\mathbf{J}+\mathbf{R})^{\vartheta+1}\right\} < \infty. \tag{23}$$

Also, we have

$$\begin{cases}\mathbb{L}(-\ln\mathbf{S}) = -\dfrac{\Lambda}{\mathbf{S}} - \varphi_2(1-\vartheta)\dfrac{\mathbf{Q}}{\mathbf{S}} - \xi\dfrac{\mathbf{R}}{\mathbf{S}} + (\psi\mathbf{I} + \chi) + \dfrac{\wp_1^2}{2},\\ \mathbb{L}(-\ln\mathbf{E}) = -\dfrac{\psi\mathbf{IS}}{\mathbf{E}} + (\eta_1 + \eta_2 + \chi) + \dfrac{\wp_2^2}{2},\\ \mathbb{L}(-\ln\mathbf{Q}) = -\dfrac{\eta_2\mathbf{E}}{\mathbf{Q}} + (\varphi_2 + \chi) + \dfrac{\wp_3^2}{2},\\ \mathbb{L}(-\ln\mathbf{I}) = -\dfrac{\eta_1\mathbf{E}}{\mathbf{I}} + (\varphi_1 + \zeta_1 + \chi) + \dfrac{\wp_4^2}{2},\\ \mathbb{L}(-\ln\mathbf{J}) = -\dfrac{\varphi_1\mathbf{I}}{\mathbf{J}} - \varphi\vartheta\dfrac{\mathbf{Q}}{\mathbf{J}} + (\zeta_2 + \chi) + \dfrac{\wp_5^2}{2},\\ \mathbb{L}(-\ln\mathbf{R}) = -\dfrac{\zeta_1\mathbf{I}}{\mathbf{R}} - \dfrac{\zeta_1\mathbf{J}}{\mathbf{R}} + (\xi + \chi) + \dfrac{\wp_6^2}{2}.\end{cases} \tag{24}$$

Utilizing (21)–(24), we then find that

$$\begin{aligned}\mathbb{L}\mathscr{V} &\leq -5(\wp_1^8)(\mathbb{R}_0^{s^{1/5}} - 1) - \frac{\psi}{\varphi_1}\mathbf{I} - \frac{\wp_1^2\varphi_2\vartheta}{2(\chi+\xi+\wp_5^2)}\mathbf{Q} + \mathbb{C}_0 - \frac{\Lambda}{\mathbf{S}}\\ &\quad - \frac{1}{2}\varrho(\mathbf{S}^{\vartheta+1} + \mathbf{E}^{\vartheta+1} + \mathbf{Q}^{\vartheta+1} + \mathbf{I}^{\vartheta+1} + \mathbf{J}^{\vartheta+1} + \mathbf{R}^{\vartheta+1})\\ &\quad + \frac{\wp_1^2}{2} - \frac{\psi\mathbf{IS}}{\mathbf{E}} + (\eta_1+\eta_2+\chi) + \frac{\wp_2^2}{2} - \frac{\eta_2\mathbf{E}}{\mathbf{Q}} + (\varphi_2+\chi) + \frac{\wp_3^2}{2} - \frac{\varphi_1\mathbf{I}}{\mathbf{J}} - \varphi\vartheta\frac{\mathbf{Q}}{\mathbf{J}} + (\zeta_2+\chi) + \frac{\wp_5^2}{2}\\ &\quad - \frac{\zeta_1\mathbf{I}}{\mathbf{R}} - \frac{\zeta_1\mathbf{J}}{\mathbf{R}} + (\xi+\chi) + \frac{\wp_6^2}{2} - \frac{\eta_1\mathbf{E}}{\mathbf{I}} + (\varphi_1+\zeta_1+\chi) + \frac{\wp_4^2}{2}\\ &\leq -5(\wp_1^8)(\mathbb{R}_0^{s^{1/5}} - 1) - \frac{\psi}{\varphi_1}\mathbf{I} - \frac{\wp_1^2\varphi_2\vartheta}{2(\chi+\xi+\wp_5^2)}\mathbf{Q} + \mathbb{C}_0 - \frac{\Lambda}{\mathbf{S}}\end{aligned}$$

$$-\frac{1}{2}\varrho(\mathbf{S}^{\vartheta+1}+\mathbf{E}^{\vartheta+1}+\mathbf{Q}^{\vartheta+1}+\mathbf{I}^{\vartheta+1}+\mathbf{J}^{\vartheta+1}+\mathbf{R}^{\vartheta+1})$$
$$+\frac{\wp_1^2+\wp_2^2+\wp_3^2+\wp_4^2+\wp_5^2+\wp_6^2}{2}-\frac{\psi\mathbf{IS}}{\mathbf{E}}+(\eta_1+\eta_2+\varphi_2+\zeta_2+\xi+\varphi_1+\zeta_1+5\chi)$$
$$-\frac{\eta_2\mathbf{E}}{\mathbf{Q}}-\frac{\varphi_1\mathbf{I}}{\mathbf{J}}-\varphi\vartheta\frac{\mathbf{Q}}{\mathbf{J}}-\frac{\zeta_1\mathbf{I}}{\mathbf{R}}-\frac{\zeta_1\mathbf{J}}{\mathbf{R}}-\frac{\eta_1\mathbf{E}}{\mathbf{I}}. \tag{25}$$

We describe it for simplicity as

$$\mathscr{H}_1=\sup\left\{-5(\wp_1^8)(\mathbb{R}_0^{S^{1/5}}-1)-\frac{\psi}{\varphi_1}\mathbf{I}-\frac{\wp_1^2\varphi_2\vartheta}{2(\chi+\xi+\wp_5^2)}\mathbf{Q}-\frac{1}{5}\varrho\mathbf{J}^{\vartheta+1}\right\}<\infty. \tag{26}$$

and

$$\mathscr{H}_2=\mathbb{C}_0+\frac{\wp_1^2+\wp_2^2+\wp_3^2+\wp_4^2+\wp_5^2+\wp_6^2}{2}+(\eta_1+\eta_2+\varphi_2+\zeta_2+\xi+\varphi_1+\zeta_1+5\chi). \tag{27}$$

We can now design a bounded compact region $\mathscr{G}_\epsilon$ that fulfills the assumption **(ii)** in Lemma 3.2. To do this, we construct a compact set as follows:

$$\mathscr{G}_\epsilon=\Big\{(\mathbf{S},\mathbf{E},\mathbf{Q},\mathbf{I},\mathbf{J},\mathbf{R})\in\mathbb{R}_+^6:\mathbf{S}\in[\epsilon,1/\epsilon],\mathbf{E}\in[\epsilon^3,1/\epsilon^3],\mathbf{Q}\in[\epsilon^4,1/\epsilon^4],\mathbf{I}\in[\epsilon,1/\epsilon],\mathbf{J}\in[\epsilon^2,1/\epsilon^2],$$
$$\mathbf{R}\in[\epsilon^5,1/\epsilon^5]\Big\},$$

where $\epsilon>0$ is sufficiently small constant such that

$$-5(\wp_1^8)(\mathbb{R}_0^{S^{1/5}}-1)-\frac{\psi}{\varphi_1}\epsilon-\frac{\wp_1^2\varphi_2\vartheta}{2(\chi+\xi+\wp_5^2)}\epsilon^4+\mathscr{H}_2<-1 \tag{28}$$

and

$$-\left(\frac{\Lambda}{\epsilon}\wedge\frac{\eta_2}{\epsilon^4}\wedge\frac{\varphi_1}{\epsilon}\wedge\frac{\varphi\vartheta}{\epsilon^2}\wedge\frac{\zeta_1}{\epsilon^5}\wedge\frac{\zeta_1}{\epsilon^5}\wedge\frac{\eta_1}{\epsilon}\wedge\frac{\varrho}{2\epsilon^{4(\vartheta+1)}}\wedge\frac{\varrho}{4\epsilon^{\vartheta+1}}\right)+\mathscr{H}_1+\mathscr{H}_2<-1. \tag{29}$$

For simplicity, we can subdivide $\mathbb{R}_+^6\setminus\mathscr{G}_\epsilon$ into the following regions, where

$$\mathscr{G}_1=\big\{(\mathbf{S},\mathbf{E},\mathbf{Q},\mathbf{I},\mathbf{J},\mathbf{R})\in\mathbb{R}_+^6\mid\mathbf{S}\in(0,\epsilon)\big\},\quad\mathscr{G}_2=\big\{(\mathbf{S},\mathbf{E},\mathbf{Q},\mathbf{I},\mathbf{J},\mathbf{R})\in\mathbb{R}_+^6\mid\mathbf{E}\in(0,\epsilon)\big\}$$
$$\mathscr{G}_3=\big\{(\mathbf{S},\mathbf{E},\mathbf{Q},\mathbf{I},\mathbf{J},\mathbf{R})\in\mathbb{R}_+^6\mid\mathbf{Q}\in(0,\epsilon^2),\ \ \mathbf{I}\geq\epsilon\big\},\quad\mathscr{G}_4=\big\{(\mathbf{S},\mathbf{E},\mathbf{Q},\mathbf{I},\mathbf{J},\mathbf{R})\in\mathbb{R}_+^6\mid\mathbf{E}\in(0,\epsilon^3)\mathbf{J}\geq\epsilon\big\}$$
$$\mathscr{G}_5=\big\{(\mathbf{S},\mathbf{E},\mathbf{Q},\mathbf{I},\mathbf{J},\mathbf{R})\in\mathbb{R}_+^6\mid\mathbf{J}>\frac{1}{\epsilon^2}\big\},\quad\mathscr{G}_6=\big\{(\mathbf{S},\mathbf{E},\mathbf{Q},\mathbf{I},\mathbf{J},\mathbf{R})\in\mathbb{R}_+^6\mid\mathbf{R}\in(0,\epsilon^3)\mathbf{J}\geq\epsilon\big\}$$
$$\mathscr{G}_7=\big\{(\mathbf{S},\mathbf{E},\mathbf{Q},\mathbf{I},\mathbf{J},\mathbf{R})\in\mathbb{R}_+^6\mid\mathbf{S}>\frac{1}{\epsilon}\big\},\quad\mathscr{G}_8=\big\{(\mathbf{S},\mathbf{E},\mathbf{Q},\mathbf{I},\mathbf{J},\mathbf{R})\in\mathbb{R}_+^6\mid\mathbf{E}>\frac{1}{\epsilon^3}\big\}$$
$$\mathscr{G}_9=\big\{(\mathbf{S},\mathbf{E},\mathbf{Q},\mathbf{I},\mathbf{J},\mathbf{R})\in\mathbb{R}_+^6\mid\mathbf{Q}>\frac{1}{\epsilon^4}\big\},\quad\mathscr{G}_{10}=\big\{(\mathbf{S},\mathbf{E},\mathbf{Q},\mathbf{I},\mathbf{J},\mathbf{R})\in\mathbb{R}_+^6\mid\mathbf{R}>\frac{1}{\epsilon^5}\big\}.$$

Evidently, $\mathbb{R}_+^6\mid\mathscr{G}_\epsilon=\bigcup_{\iota=1}^{10}\mathscr{G}_\iota$. Following that, we shall demonstrate that $\mathbb{L}\mathscr{V}(\mathbf{S},\mathbf{E},\mathbf{Q},\mathbf{I},\mathbf{J},\mathbf{R})\leq-1$ for each $(\mathbf{S},\mathbf{E},\mathbf{Q},\mathbf{I},\mathbf{J},\mathbf{R})\in\mathbb{R}_+^6\mid\mathscr{G}_\epsilon$, which is analogous to demonstrating it on the ten regions listed above.

Case I. For each $(\mathbf{S},\mathbf{E},\mathbf{Q},\mathbf{I},\mathbf{J},\mathbf{R})\in\mathscr{G}_1$, then (25) states that

$$\begin{aligned}\mathbb{L}\mathscr{V}&\le -5(\wp_1^8)(\mathbb{R}_0^{s^{1/5}}-1)+\mathbb{C}_0-\frac{\Lambda}{\mathbf{S}}+\frac{\wp_1^2\vee\wp_2^2\vee\wp_3^2\vee\wp_4^2\vee\wp_5^2\vee\wp_6^2}{2}\\&+(\eta_1+\eta_2+\varphi_2+\zeta_2+\xi+\varphi_1+\zeta_1+5\chi)-\frac{1}{2}\varrho\mathbf{J}^{\vartheta+1}\\&\le-\frac{\Lambda}{\epsilon}+\mathscr{H}_1+\mathscr{H}_2.\end{aligned}\tag{30}$$

Case II. For each $(\mathbf{S},\mathbf{E},\mathbf{Q},\mathbf{I},\mathbf{J},\mathbf{R})\in\mathscr{G}_2$, then (25) states that

$$\begin{aligned}\mathbb{L}\mathscr{V}&\le -5(\wp_1^8)(\mathbb{R}_0^{s^{1/5}}-1)+\mathbb{C}_0+\frac{\wp_1^2\vee\wp_2^2\vee\wp_3^2\vee\wp_4^2\vee\wp_5^2\vee\wp_6^2}{2}-\frac{\psi\mathbf{IS}}{\mathbf{E}}\\&+(\eta_1+\eta_2+\varphi_2+\zeta_2+\xi+\varphi_1+\zeta_1+5\chi)\\&-\frac{\eta_2\mathbf{E}}{\mathbf{Q}}-\frac{\eta_1\mathbf{E}}{\mathbf{I}}\\&\le-\frac{\psi\mathbf{IS}}{\epsilon^2}+\mathscr{H}_1+\mathscr{H}_2,\end{aligned}\tag{31}$$

Case III. For each $(\mathbf{S},\mathbf{E},\mathbf{Q},\mathbf{I},\mathbf{J},\mathbf{R})\in\mathscr{G}_3$, then (25) states that

$$\begin{aligned}\mathbb{L}\mathscr{V}&\le -5(\wp_1^8)(\mathbb{R}_0^{s^{1/5}}-1)-\frac{\wp_1^2\varphi_2\vartheta}{2(\chi+\xi+\wp_5^2)}\mathbf{Q}+\mathbb{C}_0-\frac{1}{2}\varrho(\mathbf{J}^{\vartheta+1})+\frac{\wp_1^2\vee\wp_2^2\vee\wp_3^2\vee\wp_4^2\vee\wp_5^2\vee\wp_6^2}{2}\\&+(\eta_1+\eta_2+\varphi_2+\zeta_2+\xi+\varphi_1+\zeta_1+5\chi)-\frac{\eta_2\mathbf{E}}{\mathbf{Q}}\\&\le -5(\wp_1^8)(\mathbb{R}_0^{s^{1/5}}-1)-\frac{\wp_1^2\varphi_2\vartheta}{2(\chi+\xi+\wp_5^2)}\epsilon^4+\mathscr{H}_2.\end{aligned}\tag{32}$$

Case IV. For each $(\mathbf{S},\mathbf{E},\mathbf{Q},\mathbf{I},\mathbf{J},\mathbf{R})\in\mathscr{G}_4$, then (25) states that

$$\begin{aligned}\mathbb{L}\mathscr{V}&\le -5(\wp_1^8)(\mathbb{R}_0^{s^{1/5}}-1)-\frac{\psi}{\varphi_1}\mathbf{I}+\mathbb{C}_0-\frac{\Lambda}{\mathbf{S}}-\frac{1}{2}\varrho(\mathbf{J}^{\vartheta+1})+\frac{\wp_1^2\vee\wp_2^2\vee\wp_3^2\vee\wp_4^2\vee\wp_5^2\vee\wp_6^2}{2}-\frac{\psi\mathbf{IS}}{\mathbf{E}}\\&+(\eta_1+\eta_2+\varphi_2+\zeta_2+\xi+\varphi_1+\zeta_1+5\chi)-\frac{\eta_1\mathbf{E}}{\mathbf{I}}\\&\le-\frac{\eta_1}{\epsilon}+\mathscr{H}_1+\mathscr{H}_2.\end{aligned}\tag{33}$$

Case V. For each $(\mathbf{S},\mathbf{E},\mathbf{Q},\mathbf{I},\mathbf{J},\mathbf{R})\in\mathscr{G}_5$, then (25) states that

$$\begin{aligned}\mathbb{L}\mathscr{V}&\le -5(\wp_1^8)(\mathbb{R}_0^{s^{1/5}}-1)-\frac{\wp_1^2\varphi_2\vartheta}{2(\chi+\xi+\wp_5^2)}\mathbf{Q}+\mathbb{C}_0-\frac{1}{2}\varrho(\mathbf{J}^{\vartheta+1})+\frac{\wp_1^2\vee\wp_2^2\vee\wp_3^2\vee\wp_4^2\vee\wp_5^2\vee\wp_6^2}{2}\\&+(\eta_1+\eta_2+\varphi_2+\zeta_2+\xi+\varphi_1+\zeta_1+5\chi)\\&-\frac{\varphi_1\mathbf{I}}{\mathbf{J}}-\varphi\vartheta\frac{\mathbf{Q}}{\mathbf{J}}\\&\le-\frac{\varphi_1}{\epsilon^2}-\varphi\vartheta\frac{1}{\epsilon^2}+\mathscr{H}_1+\mathscr{H}_2.\end{aligned}\tag{34}$$

Case VI. For each $(\mathbf{S},\mathbf{E},\mathbf{Q},\mathbf{I},\mathbf{J},\mathbf{R}) \in \mathscr{G}_6$, then (25) states that

$$\begin{aligned}
\mathbb{L}\mathscr{V} &\leq -5(\wp_1^8)(\mathbb{R}_0^{s^{1/5}} - 1) - \frac{\wp_1^2\varphi_2\vartheta}{2(\chi+\xi+\wp_5^2)}\mathbf{Q} + \mathbb{C}_0 - \frac{\Lambda}{\mathbf{S}} - \frac{1}{2}\varrho(\mathbf{J}^{\vartheta+1}) + \frac{\wp_1^2 \vee \wp_2^2 \vee \wp_3^2 \vee \wp_4^2 \vee \wp_5^2 \vee \wp_6^2}{2} \\
&\quad + (\eta_1+\eta_2+\varphi_2+\zeta_2+\xi+\varphi_1+\zeta_1+5\chi) \\
&\leq \frac{1}{2}\varrho\frac{1}{\epsilon^{\vartheta+1}} + \mathscr{H}_1 + \mathscr{H}_2.
\end{aligned} \tag{35}$$

Case VII. For each $(\mathbf{S},\mathbf{E},\mathbf{Q},\mathbf{I},\mathbf{J},\mathbf{R}) \in \mathscr{G}_7$, then (25) states that

$$\begin{aligned}
\mathbb{L}\mathscr{V} &\leq -5(\wp_1^8)(\mathbb{R}_0^{s^{1/5}} - 1) - \frac{\wp_1^2\varphi_2\vartheta}{2(\chi+\xi+\wp_5^2)}\mathbf{Q} + \mathbb{C}_0 - \frac{1}{2}\varrho(\mathbf{J}^{\vartheta+1}) + \frac{1}{2}\varrho(\mathbf{S}^{\vartheta+1}) \\
&\quad + \frac{\wp_1^2 \vee \wp_2^2 \vee \wp_3^2 \vee \wp_4^2 \vee \wp_5^2 \vee \wp_6^2}{2} + (\eta_1+\eta_2+\varphi_2+\zeta_2+\xi+\varphi_1+\zeta_1+5\chi) \\
&\leq -\frac{1}{2}\varrho\frac{1}{\epsilon^{3(\vartheta+1)}} + \mathscr{H}_1 + \mathscr{H}_2.
\end{aligned} \tag{36}$$

Case VIII. For each $(\mathbf{S},\mathbf{E},\mathbf{Q},\mathbf{I},\mathbf{J},\mathbf{R}) \in \mathscr{G}_8$, then (25) states that

$$\begin{aligned}
\mathbb{L}\mathscr{V} &\leq -5(\wp_1^8)(\mathbb{R}_0^{s^{1/5}} - 1) - \frac{\wp_1^2\varphi_2\vartheta}{2(\chi+\xi+\wp_5^2)}\mathbf{Q} + \mathbb{C}_0 - \frac{1}{2}\varrho(\mathbf{J}^{\vartheta+1}) + \frac{1}{2}\varrho(\mathbf{E}^{\vartheta+1}) \\
&\quad + \frac{\wp_1^2 \vee \wp_2^2 \vee \wp_3^2 \vee \wp_4^2 \vee \wp_5^2 \vee \wp_6^2}{2} + (\eta_1+\eta_2+\varphi_2+\zeta_2+\xi+\varphi_1+\zeta_1+5\chi) \\
&\leq -\frac{1}{2}\varrho\frac{1}{\epsilon^{4(\vartheta+1)}} + \mathscr{H}_1 + \mathscr{H}_2.
\end{aligned} \tag{37}$$

Case IX. For each $(\mathbf{S},\mathbf{E},\mathbf{Q},\mathbf{I},\mathbf{J},\mathbf{R}) \in \mathscr{G}_9$, then (25) states that

$$\begin{aligned}
\mathbb{L}\mathscr{V} &\leq -5(\wp_1^8)(\mathbb{R}_0^{s^{1/5}} - 1) - \frac{\wp_1^2\varphi_2\vartheta}{2(\chi+\xi+\wp_5^2)}\mathbf{Q} + \mathbb{C}_0 - \frac{1}{2}\varrho(\mathbf{J}^{\vartheta+1}) + \frac{1}{2}\varrho(\mathbf{Q}^{\vartheta+1}) \\
&\quad + \frac{\wp_1^2 \vee \wp_2^2 \vee \wp_3^2 \vee \wp_4^2 \vee \wp_5^2 \vee \wp_6^2}{2} + (\eta_1+\eta_2+\varphi_2+\zeta_2+\xi+\varphi_1+\zeta_1+5\chi) \\
&\leq -\frac{1}{2}\varrho\frac{1}{\epsilon^{(\vartheta+1)}} + \mathscr{H}_1 + \mathscr{H}_2.
\end{aligned} \tag{38}$$

Case X. For each $(\mathbf{S},\mathbf{E},\mathbf{Q},\mathbf{I},\mathbf{J},\mathbf{R}) \in \mathscr{G}_2$, then (25) states that

$$\begin{aligned}
\mathbb{L}\mathscr{V} &\leq -5(\wp_1^8)(\mathbb{R}_0^{s^{1/5}} - 1) - \frac{\wp_1^2\varphi_2\vartheta}{2(\chi+\xi+\wp_5^2)}\mathbf{Q} + \mathbb{C}_0 - \frac{1}{2}\varrho(\mathbf{J}^{\vartheta+1}) + \frac{1}{2}\varrho(\mathbf{R}^{\vartheta+1}) \\
&\quad + \frac{\wp_1^2 \vee \wp_2^2 \vee \wp_3^2 \vee \wp_4^2 \vee \wp_5^2 \vee \wp_6^2}{2} + (\eta_1+\eta_2+\varphi_2+\zeta_2+\xi+\varphi_1+\zeta_1+5\chi) \\
&\leq -\frac{1}{2}\varrho\frac{1}{\epsilon^{2(\vartheta+1)}} + \mathscr{H}_1 + \mathscr{H}_2.
\end{aligned} \tag{39}$$

As a result of (26)–(39), we have

$$\mathbb{L}\mathscr{V} < -1, \quad \forall(\mathbf{S}, \mathbf{E}, \mathbf{Q}, \mathbf{I}, \mathbf{J}, \mathbf{R}) \in \mathbb{R}^5_+ \mid \mathscr{G}_\epsilon. \tag{40}$$

This demonstrates that requirement **(ii)** is satisfied. As a result of the verification of the requirements in Lemma 3.2, the evidence is fulfilled.

4 Numerical Procedures of COVID-19 Framework for Various Fractional Derivative Operators

4.1 Caputo Fractional Derivative Operator

In this part, we will investigate the dynamical behaviour of COVID-19 transmission, which displays three patterns for a country, involving classical, index-law, and eventually stochastic processes. In this scenario, if we define $\mathbb{T}$ as the final time of transmission, that is, the penultimate time when a secondary outbreak occurs, then the mathematical framework will be developed using the classical derivative formulation in the first round, then the index-law kernel in the second step, and finally the stochastic environment in the later phases. Following that, the mathematical formalism that explains this phenomenon is offered as

$$\begin{cases} \dfrac{d\mathbf{S}}{d\mathbf{t}} = \Lambda + \varphi_2(1-\vartheta)\mathbf{Q} + \xi\mathbf{R} - (\psi\mathbf{I} + \chi)\mathbf{S}, \\ \dfrac{d\mathbf{E}}{d\mathbf{t}} = \psi\mathbf{IS} - (\eta_1 + \eta_2 + \chi)\mathbf{E}, \\ \dfrac{d\mathbf{Q}}{d\mathbf{t}} = \eta_2\mathbf{E} - (\chi + \varphi_2)\mathbf{Q}, \quad if \quad 0 \le \mathbf{t} \le \mathbb{T}_1, \\ \dfrac{d\mathbf{I}}{d\mathbf{t}} = \eta_1\mathbf{E} - (\varphi_1 + \zeta_1 + \chi)\mathbf{I}, \\ \dfrac{d\mathbf{J}}{d\mathbf{t}} = \varphi_1\mathbf{I} + \varphi_2\vartheta\mathbf{Q} - (\chi + \zeta_2)\mathbf{J}, \\ \dfrac{d\mathbf{R}}{d\mathbf{t}} = \zeta_1\mathbf{I} + \zeta_2\mathbf{J} - (\xi + \chi)\mathbf{R}, \end{cases} \tag{41}$$

$$\begin{cases} {}_0^c\mathbf{D}_\mathbf{t}^\beta\mathbf{S}(\mathbf{t}) = \Lambda + \varphi_2(1-\vartheta)\mathbf{Q} + \xi\mathbf{R} - (\psi\mathbf{I} + \chi)\mathbf{S}, \\ {}_0^c\mathbf{D}_\mathbf{t}^\beta\mathbf{E}(\mathbf{t}) = \psi\mathbf{IS} - (\eta_1 + \eta_2 + \chi)\mathbf{E}, \\ {}_0^c\mathbf{D}_\mathbf{t}^\beta\mathbf{Q}(\mathbf{t}) = \eta_2\mathbf{E} - (\chi + \varphi_2)\mathbf{Q}, \quad if \quad \mathbb{T}_1 \le \mathbf{t} \le \mathbb{T}_2, \\ {}_0^c\mathbf{D}_\mathbf{t}^\beta\mathbf{I}(\mathbf{t}) = \eta_1\mathbf{E} - (\varphi_1 + \zeta_1 + \chi)\mathbf{I}, \\ {}_0^c\mathbf{D}_\mathbf{t}^\beta\mathbf{J}(\mathbf{t}) = \varphi_1\mathbf{I} + \varphi_2\vartheta\mathbf{Q} - (\chi + \zeta_2)\mathbf{J}, \\ {}_0^c\mathbf{D}_\mathbf{t}^\beta\mathbf{R}(\mathbf{t}) = \zeta_1\mathbf{I} + \zeta_2\mathbf{J} - (\xi + \chi)\mathbf{R}, \end{cases} \tag{42}$$

$$\begin{cases} d\mathbf{S}(\mathbf{t}) = \big(\Lambda + \varphi_2(1-\vartheta)\mathbf{Q} + \xi\mathbf{R} - (\psi\mathbf{I} + \chi)\mathbf{S}\big) + \wp_1\mathbf{S}(\mathbf{t})d\mathscr{W}_1(\mathbf{t}), \\ d\mathbf{E}(\mathbf{t}) = \big(\psi\mathbf{IS} - (\eta_1 + \eta_2 + \chi)\mathbf{E}\big) + \wp_2\mathbf{E}(\mathbf{t})d\mathscr{W}_2(\mathbf{t}), \\ d\mathbf{Q}(\mathbf{t}) = \big(\eta_2\mathbf{E} - (\chi + \varphi_2)\mathbf{Q}\big) + \wp_3\mathbf{Q}(\mathbf{t})d\mathscr{W}_3(\mathbf{t}), \quad \textit{if} \quad \mathbb{T}_2 \le \mathbf{t} \le \mathbb{T}, \\ d\mathbf{I}(\mathbf{t}) = \big(\eta_1\mathbf{E} - (\varphi_1 + \zeta_1 + \chi)\mathbf{I}\big) + \wp_4\mathbf{I}(\mathbf{t})d\mathscr{W}_4(\mathbf{t}), \\ d\mathbf{J}(\mathbf{t}) = \big(\varphi_1\mathbf{I} + \varphi_2\vartheta\mathbf{Q} - (\chi + \zeta_2)\mathbf{J}\big) + \wp_5\mathbf{J}(\mathbf{t})d\mathscr{W}_5(\mathbf{t}), \\ d\mathbf{R}(\mathbf{t}) = \big(\zeta_1\mathbf{I} + \zeta_2\mathbf{J} - (\xi + \chi)\mathbf{R}\big) + \wp_6\mathbf{R}(\mathbf{t})d\mathscr{W}_6(\mathbf{t}), \end{cases} \tag{43}$$

Here, we apply the technique described in [44] for the scenario of Caputo's derivative to analyze quantitatively the piecewise structure (41)–(43). We commence the technique as follows:

$$\begin{cases} \dfrac{d\Phi_\kappa(\mathbf{t})}{d\mathbf{t}} = \Upsilon(\mathbf{t}, \Phi_\kappa). \ \ \Phi_\kappa(0) = \Phi_{\kappa,0}, \ \ \kappa = 1, 2, \ldots, n_1 & \textit{if} \ \ \mathbf{t} \in [0, \mathbb{T}_1], \\ {}^{c}_{\mathbb{T}_1}\mathbf{D}^{\beta}_{\mathbf{t}}\Phi_\kappa(\mathbf{t}) = \Upsilon(\mathbf{t}, \Phi_\kappa), \ \ \Phi_\kappa(\mathbb{T}_1) = \Phi_{\kappa,1}, & \textit{if} \ \ \mathbf{t} \in [\mathbb{T}_1, \mathbb{T}_2], \\ d\Phi_\kappa(\mathbf{t}) = \Upsilon(\mathbf{t}, \Phi_\kappa)d\mathbf{t} + \wp_\kappa\Phi_\kappa d\mathscr{W}_\kappa(\mathbf{t}), \ \ \Phi_\kappa(\mathbb{T}_2) = \Phi_{\kappa,2}, & \textit{if} \ \ \mathbf{t} \in [\mathbb{T}_2, \mathbb{T}]. \end{cases}$$

It follows that

$$\Phi^{\mathbf{r}}_\kappa = \begin{cases} \Phi_\kappa(0) + \sum\limits_{\Bbbk=2}^{\mathbf{r}} \left\{ \dfrac{23}{12}\Upsilon(\mathbf{t}_\Bbbk, \Phi^\Bbbk)\Delta\mathbf{t} - \dfrac{4}{3}\Upsilon(\mathbf{t}_{\Bbbk-1}, \Phi^{\Bbbk-1})\Delta\mathbf{t} + \dfrac{5}{12}\Upsilon(\mathbf{t}_{\Bbbk-2}, \Phi^{\Bbbk-2})\Delta\mathbf{t} \right\}, \quad \mathbf{t} \in [0, \mathbb{T}_\nVdash]. \\ \Phi_\kappa(\mathbb{T}_1) + \dfrac{(\Delta\mathbf{t})^{\beta-1}}{\Gamma(\beta+1)} \sum\limits_{\Bbbk=2}^{\mathbf{r}} \Upsilon(\mathbf{t}_{\Bbbk-2}, \Phi^{\Bbbk-2})\,\Xi_1 \\ \quad + \dfrac{(\Delta\mathbf{t})^{\beta-1}}{\Gamma(\beta+2)} \sum\limits_{\Bbbk=2}^{\mathbf{r}} \left\{ \Upsilon(\mathbf{t}_{\Bbbk-1}, \Phi^{\Bbbk-1}) - \Upsilon(\mathbf{t}_{\Bbbk-2}, \Phi^{\Bbbk-2}) \right\} \Xi_2 \\ \quad + \dfrac{\beta(\Delta\mathbf{t})^{\beta-1}}{2\Gamma(\beta+3)} \sum\limits_{\Bbbk=2}^{\mathbf{r}} \left\{ \Upsilon(\mathbf{t}_\Bbbk, \Phi^\Bbbk) - 2\Upsilon(\mathbf{t}_{\Bbbk-1}, \Phi^{\Bbbk-1}) + \Upsilon(\mathbf{t}_{\Bbbk-2}, \Phi^{\Bbbk-2}) \right\} \Xi_3, \quad \mathbf{t} \in [\mathbb{T}_1, \mathbb{T}_2], \\ \Phi_\kappa(\mathbb{T}_2) + \sum\limits_{\Bbbk=\mathbf{r}+3}^{n_1} \left\{ \dfrac{5}{12}\Upsilon(\mathbf{t}_{\Bbbk-2}, \Phi^{\Bbbk-2})\Delta\mathbf{t} - \dfrac{4}{3}\Upsilon(\mathbf{t}_{\Bbbk-1}, \Phi^{\Bbbk-1})\Delta\mathbf{t} + \dfrac{23}{12}\Upsilon(\mathbf{t}_\Bbbk, \Phi^\Bbbk)\Delta\mathbf{t} \right\} \\ \quad + \sum\limits_{\Bbbk=\mathbf{r}+3}^{n_1} \left\{ \dfrac{5}{12}\big(B(\mathbf{t}_{\Bbbk-1}) - B(\mathbf{t}_{\Bbbk-2})\big)\wp\Phi^{\Bbbk-2} - \dfrac{4}{3}\big(B(\mathbf{t}_\Bbbk) - B(\mathbf{t}_{\Bbbk-1})\big)\wp\Phi^{\Bbbk-1} \right. \\ \quad \left. + \dfrac{23}{12}\big(B(\mathbf{t}_{\Bbbk+1}) - B(\mathbf{t}_\Bbbk)\big)\wp\Phi^\Bbbk \right\}, \quad \mathbf{t} \in [\mathbb{T}_2, \mathbb{T}], \end{cases}$$

where

$$\Xi_1 := (\mathbf{r} - \Bbbk - 1)^\beta - (\mathbf{r} - \Bbbk)^\beta, \tag{44}$$

$$\Xi_2 := (\mathbf{r} - \Bbbk + 1)^\beta(\mathbf{r} - \Bbbk + 2\beta + 3) - (\mathbf{r} - \Bbbk)^\beta(\mathbf{r} - \Bbbk + 3\beta + 3) \tag{45}$$

and

$$\Xi_3 := \begin{cases} (\mathbf{r} - \mathbb{k} + 1)^{\beta}\Big(2(\mathbf{r} - \mathbb{k})^2 + (3\beta + 10)(\mathbf{r} - \mathbb{k}) + 2\beta^2 + 9\beta + 12\Big) \\ \quad +(\mathbf{r} - \mathbb{k})^{\beta}\Big(2(\mathbf{r} - \mathbb{k})^2 + (5\beta + 10)(\mathbf{r} - \mathbb{k}) + 6\beta^2 + 18\beta + 12\Big). \end{cases} \tag{46}$$

4.2 Caputo-Fabrizio Fractional Derivative Operator

In this section, we will examine the system dynamics of COVID-19 propagation, which shows three phases for a particular country, comprising classical, exponential decay law, and finally stochastic mechanisms. If we describe $\mathbb{T}$ as the concluding time of transmitted, that is, the final time when a secondary epidemic appears, then the mathematical structure will be formed in the first round using the classical derivative implementation, then the exponential decay kernel in the second step, and eventually the stochastic environment in the subsequent periods. Regarding that, the mathematical approach used to illustrate this occurrence is presented as follows:

$$\begin{cases} \dfrac{d\mathbf{S}}{d\mathbf{t}} = \Lambda + \varphi_2(1 - \vartheta)\mathbf{Q} + \xi\mathbf{R} - (\psi\mathbf{I} + \chi)\mathbf{S}, \\ \dfrac{d\mathbf{E}}{d\mathbf{t}} = \psi\mathbf{IS} - (\eta_1 + \eta_2 + \chi)\mathbf{E}, \\ \dfrac{d\mathbf{Q}}{d\mathbf{t}} = \eta_2\mathbf{E} - (\chi + \varphi_2)\mathbf{Q}, \quad \mathit{if} \quad 0 \le \mathbf{t} \le \mathbb{T}_1, \\ \dfrac{d\mathbf{I}}{d\mathbf{t}} = \eta_1\mathbf{E} - (\varphi_1 + \zeta_1 + \chi)\mathbf{I}, \\ \dfrac{d\mathbf{J}}{d\mathbf{t}} = \varphi_1\mathbf{I} + \varphi_2\vartheta\mathbf{Q} - (\chi + \zeta_2)\mathbf{J}, \\ \dfrac{d\mathbf{R}}{d\mathbf{t}} = \zeta_1\mathbf{I} + \zeta_2\mathbf{J} - (\xi + \chi)\mathbf{R}, \end{cases} \tag{47}$$

$$\begin{cases} {}_0^{CF}\mathbf{D}_{\mathbf{t}}^{\beta}\mathbf{S}(\mathbf{t}) = \Lambda + \varphi_2(1 - \vartheta)\mathbf{Q} + \xi\mathbf{R} - (\psi\mathbf{I} + \chi)\mathbf{S}, \\ {}_0^{CF}\mathbf{D}_{\mathbf{t}}^{\beta}\mathbf{E}(\mathbf{t}) = \psi\mathbf{IS} - (\eta_1 + \eta_2 + \chi)\mathbf{E}, \\ {}_0^{CF}\mathbf{D}_{\mathbf{t}}^{\beta}\mathbf{Q}(\mathbf{t}) = \eta_2\mathbf{E} - (\chi + \varphi_2)\mathbf{Q}, \quad \mathit{if} \quad \mathbb{T}_1 \le \mathbf{t} \le \mathbb{T}_2, \\ {}_0^{CF}\mathbf{D}_{\mathbf{t}}^{\beta}\mathbf{I}(\mathbf{t}) = \eta_1\mathbf{E} - (\varphi_1 + \zeta_1 + \chi)\mathbf{I}, \\ {}_0^{CF}\mathbf{D}_{\mathbf{t}}^{\beta}\mathbf{J}(\mathbf{t}) = \varphi_1\mathbf{I} + \varphi_2\vartheta\mathbf{Q} - (\chi + \zeta_2)\mathbf{J}, \\ {}_0^{CF}\mathbf{D}_{\mathbf{t}}^{\beta}\mathbf{R}(\mathbf{t}) = \zeta_1\mathbf{I} + \zeta_2\mathbf{J} - (\xi + \chi)\mathbf{R}, \end{cases} \tag{48}$$

$$\begin{cases} d\mathbf{S}(\mathbf{t}) = \left(\Lambda + \varphi_2(1-\vartheta)\mathbf{Q} + \xi\mathbf{R} - (\psi\mathbf{I} + \chi)\mathbf{S}\right) + \wp_1\mathbf{S}(\mathbf{t})d\mathscr{W}_1(\mathbf{t}), \\ d\mathbf{E}(\mathbf{t}) = \left(\psi\mathbf{IS} - (\eta_1 + \eta_2 + \chi)\mathbf{E}\right) + \wp_2\mathbf{E}(\mathbf{t})d\mathscr{W}_2(\mathbf{t}), \\ d\mathbf{Q}(\mathbf{t}) = \left(\eta_2\mathbf{E} - (\chi + \varphi_2)\mathbf{Q}\right) + \wp_3\mathbf{Q}(\mathbf{t})d\mathscr{W}_3(\mathbf{t}), \quad \mathit{if} \quad \mathbb{T}_2 \le \mathbf{t} \le \mathbb{T}, \\ d\mathbf{I}(\mathbf{t}) = \left(\eta_1\mathbf{E} - (\varphi_1 + \zeta_1 + \chi)\mathbf{I}\right) + \wp_4\mathbf{I}(\mathbf{t})d\mathscr{W}_4(\mathbf{t}), \\ d\mathbf{J}(\mathbf{t}) = \left(\varphi_1\mathbf{I} + \varphi_2\vartheta\mathbf{Q} - (\chi + \zeta_2)\mathbf{J}\right) + \wp_5\mathbf{J}(\mathbf{t})d\mathscr{W}_5(\mathbf{t}), \\ d\mathbf{R}(\mathbf{t}) = \left(\zeta_1\mathbf{I} + \zeta_2\mathbf{J} - (\xi + \chi)\mathbf{R}\right) + \wp_6\mathbf{R}(\mathbf{t})d\mathscr{W}_6(\mathbf{t}), \end{cases} \tag{49}$$

Here, we apply the technique described in [44] for the scenario of Caputo-Fabrizio derivative to analyze quantitatively the piecewise structure (47)–(49). We commence the technique as follows:

$$\begin{cases} \dfrac{d\Phi_\kappa(\mathbf{t})}{d\mathbf{t}} = \Upsilon(\mathbf{t}, \Phi_\kappa). \ \ \Phi_\kappa(0) = \Phi_{\kappa,0}, \ \ \kappa = 1, 2, \ldots, n_1 & \mathit{if} \ \ \mathbf{t} \in [0, \mathbb{T}_1], \\ {}^{CF}_{\mathbb{T}_1}\mathbf{D}^{\beta}_{\mathbf{t}}\Phi_\kappa(\mathbf{t}) = \Upsilon(\mathbf{t}, \Phi_\kappa), \ \ \Phi_\kappa(\mathbb{T}_1) = \Phi_{\kappa,1}, & \mathit{if} \ \ \mathbf{t} \in [\mathbb{T}_1, \mathbb{T}_2], \\ d\Phi_\kappa(\mathbf{t}) = \Upsilon(\mathbf{t}, \Phi_\kappa)d\mathbf{t} + \wp_\kappa\Phi_\kappa d\mathscr{W}_\kappa(\mathbf{t}), \ \ \Phi_\kappa(\mathbb{T}_2) = \Phi_{\kappa,2}, & \mathit{if} \ \ \mathbf{t} \in [\mathbb{T}_2, \mathbb{T}]. \end{cases} \tag{50}$$

It follows that

$$\Phi^{\mathbf{r}}_\kappa = \begin{cases} \Phi_\kappa(0) + \sum\limits_{\Bbbk=2}^{\mathbf{r}} \left\{ \dfrac{23}{12}\Upsilon(\mathbf{t}_\Bbbk, \Phi^\Bbbk)\Delta\mathbf{t} - \dfrac{4}{3}\Upsilon(\mathbf{t}_{\Bbbk-1}, \Phi^{\Bbbk-1})\Delta\mathbf{t} + \dfrac{5}{12}\Upsilon(\mathbf{t}_{\Bbbk-2}, \Phi^{\Bbbk-2})\Delta\mathbf{t} \right\}, \quad \mathbf{t} \in [0, \mathbb{T}_\Bbbk]. \\ \Phi_\kappa(\mathbb{T}_1) + \dfrac{1-\beta}{\mathbb{M}(\beta)}\Upsilon(\mathbf{t}_{n_1}, \Phi^{n_1}) + \dfrac{\beta}{\mathbb{M}(\beta)}\sum\limits_{\Bbbk=2}^{\mathbf{r}} \left\{ \dfrac{5}{12}\Upsilon(\mathbf{t}_{\Bbbk-2}, \Phi^{\Bbbk-2})\Delta\mathbf{t} - \dfrac{4}{3}\Upsilon(\mathbf{t}_{\Bbbk-1}, \Phi^{\Bbbk-1})\Delta\mathbf{t} \right. \\ \left. \quad + \dfrac{23}{12}\Upsilon(\mathbf{t}_\Bbbk, \Phi^\Bbbk)\Delta\mathbf{t} \right\}, \quad \mathbf{t} \in [\mathbb{T}_1, \mathbb{T}_2], \\ \Phi_\kappa(\mathbb{T}_2) + \sum\limits_{\Bbbk=\mathbf{r}+3}^{n_1} \left\{ \dfrac{5}{12}\Upsilon(\mathbf{t}_{\Bbbk-2}, \Phi^{\Bbbk-2})\Delta\mathbf{t} - \dfrac{4}{3}\Upsilon(\mathbf{t}_{\Bbbk-1}, \Phi^{\Bbbk-1})\Delta\mathbf{t} + \dfrac{23}{12}\Upsilon(\mathbf{t}_\Bbbk, \Phi^\Bbbk)\Delta\mathbf{t} \right\} \\ \quad + \sum\limits_{\Bbbk=\mathbf{r}+3}^{n_1} \left\{ \dfrac{5}{12}\big(B(\mathbf{t}_{\Bbbk-1}) - B(\mathbf{t}_{\Bbbk-2})\big)\wp\Phi^{\Bbbk-2} - \dfrac{4}{3}\big(B(\mathbf{t}_\Bbbk) - B(\mathbf{t}_{\Bbbk-1})\big)\wp\Phi^{\Bbbk-1} \right. \\ \left. \quad + \dfrac{23}{12}\big(B(\mathbf{t}_{\Bbbk+1}) - B(\mathbf{t}_\Bbbk)\big)\wp\Phi^\Bbbk \right\}, \quad \mathbf{t} \in [\mathbb{T}_2, \mathbb{T}]. \end{cases} \tag{51}$$

4.3 Atangana-Baleanu Fractional Derivative Operator

Here, we will concentrate on the dynamic behavior of COVID-19 spreading in this portion, which demonstrates three main phases for a certain region, including classical, generalized Mittag-Leffler law, and lastly, stochastic causes. If we define $\mathbb{T}$ as the final time when a secondary epidemic appears, the mathematical configuration will be constituted in the first round employing the classical derivative application, followed by the Mittag-Leffler kernel in the second step, and finally the stochastic environment in subsequent periods. In this regard, the mathematical model utilized to describe this phenomenon is as follows:

$$\begin{cases} \dfrac{d\mathbf{S}}{d\mathbf{t}} = \Lambda + \varphi_2(1-\vartheta)\mathbf{Q} + \xi\mathbf{R} - (\psi\mathbf{I} + \chi)\mathbf{S}, \\ \dfrac{d\mathbf{E}}{d\mathbf{t}} = \psi\mathbf{IS} - (\eta_1 + \eta_2 + \chi)\mathbf{E}, \\ \dfrac{d\mathbf{Q}}{d\mathbf{t}} = \eta_2\mathbf{E} - (\chi + \varphi_2)\mathbf{Q}, \quad \textit{if} \quad 0 \le \mathbf{t} \le \mathbb{T}_1 \\ \dfrac{d\mathbf{I}}{d\mathbf{t}} = \eta_1\mathbf{E} - (\varphi_1 + \zeta_1 + \chi)\mathbf{I}, \\ \dfrac{d\mathbf{J}}{d\mathbf{t}} = \varphi_1\mathbf{I} + \varphi_2\vartheta\mathbf{Q} - (\chi + \zeta_2)\mathbf{J}, \\ \dfrac{d\mathbf{R}}{d\mathbf{t}} = \zeta_1\mathbf{I} + \zeta_2\mathbf{J} - (\xi + \chi)\mathbf{R}, \end{cases} \tag{52}$$

$$\begin{cases} {}_0^{ABC}\mathbf{D}_\mathbf{t}^\beta\mathbf{S}(\mathbf{t}) = \Lambda + \varphi_2(1-\vartheta)\mathbf{Q} + \xi\mathbf{R} - (\psi\mathbf{I} + \chi)\mathbf{S}, \\ {}_0^{ABC}\mathbf{D}_\mathbf{t}^\beta\mathbf{E}(\mathbf{t}) = \psi\mathbf{IS} - (\eta_1 + \eta_2 + \chi)\mathbf{E}, \\ {}_0^{ABC}\mathbf{D}_\mathbf{t}^\beta\mathbf{Q}(\mathbf{t}) = \eta_2\mathbf{E} - (\chi + \varphi_2)\mathbf{Q}, \quad \textit{if} \quad \mathbb{T}_1 \le \mathbf{t} \le \mathbb{T}_2 \\ {}_0^{ABC}\mathbf{D}_\mathbf{t}^\beta\mathbf{I}(\mathbf{t}) = \eta_1\mathbf{E} - (\varphi_1 + \zeta_1 + \chi)\mathbf{I}, \\ {}_0^{ABC}\mathbf{D}_\mathbf{t}^\beta\mathbf{J}(\mathbf{t}) = \varphi_1\mathbf{I} + \varphi_2\vartheta\mathbf{Q} - (\chi + \zeta_2)\mathbf{J}, \\ {}_0^{ABC}\mathbf{D}_\mathbf{t}^\beta\mathbf{R}(\mathbf{t}) = \zeta_1\mathbf{I} + \zeta_2\mathbf{J} - (\xi + \chi)\mathbf{R}, \end{cases} \tag{53}$$

$$\begin{cases} d\mathbf{S}(\mathbf{t}) = \big(\Lambda + \varphi_2(1-\vartheta)\mathbf{Q} + \xi\mathbf{R} - (\psi\mathbf{I} + \chi)\mathbf{S}\big) + \wp_1\mathbf{S}(\mathbf{t})d\mathscr{W}_1(\mathbf{t}), \\ d\mathbf{E}(\mathbf{t}) = \big(\psi\mathbf{IS} - (\eta_1 + \eta_2 + \chi)\mathbf{E}\big) + \wp_2\mathbf{E}(\mathbf{t})d\mathscr{W}_2(\mathbf{t}), \\ d\mathbf{Q}(\mathbf{t}) = \big(\eta_2\mathbf{E} - (\chi + \varphi_2)\mathbf{Q}\big) + \wp_3\mathbf{Q}(\mathbf{t})d\mathscr{W}_3(\mathbf{t}), \quad \textit{if} \quad \mathbb{T}_2 \le \mathbf{t} \le \mathbb{T} \\ d\mathbf{I}(\mathbf{t}) = \big(\eta_1\mathbf{E} - (\varphi_1 + \zeta_1 + \chi)\mathbf{I}\big) + \wp_4\mathbf{I}(\mathbf{t})d\mathscr{W}_4(\mathbf{t}), \\ d\mathbf{J}(\mathbf{t}) = \big(\varphi_1\mathbf{I} + \varphi_2\vartheta\mathbf{Q} - (\chi + \zeta_2)\mathbf{J}\big) + \wp_5\mathbf{J}(\mathbf{t})d\mathscr{W}_5(\mathbf{t}), \\ d\mathbf{R}(\mathbf{t}) = \big(\zeta_1\mathbf{I} + \zeta_2\mathbf{J} - (\xi + \chi)\mathbf{R}\big) + \wp_6\mathbf{R}(\mathbf{t})d\mathscr{W}_6(\mathbf{t}), \end{cases} \tag{54}$$

Here, we apply the technique described in [44] for the scenario of Atanagan-Baleanu-Caputo derivative to analyze quantitatively the piecewise structure (52)–(54). We commence the technique as follows:

$$\begin{cases} \dfrac{d\Phi_\kappa(\mathbf{t})}{d\mathbf{t}} = \Upsilon(\mathbf{t}, \Phi_\kappa). \ \ \Phi_\kappa(0) = \Phi_{\kappa,0}, \ \ \kappa = 1, 2, \ldots, n_1 & \textit{if} \ \ \mathbf{t} \in [0, \mathbb{T}_1], \\ {}_{\mathbb{T}_1}^{ABC}\mathbf{D}_\mathbf{t}^\beta\Phi_\kappa(\mathbf{t}) = \Upsilon(\mathbf{t}, \Phi_\kappa), \ \ \Phi_\kappa(\mathbb{T}_1) = \Phi_{\kappa,1}, & \textit{if} \ \ \mathbf{t} \in [\mathbb{T}_1, \mathbb{T}_2], \\ d\Phi_\kappa(\mathbf{t}) = \Upsilon(\mathbf{t}, \Phi_\kappa)dt + \wp_\kappa\Phi_\kappa d\mathscr{W}_\kappa(\mathbf{t}), \ \ \Phi_\kappa(\mathbb{T}_2) = \Phi_{\kappa,2}, & \textit{if} \ \ \mathbf{t} \in [\mathbb{T}_2, \mathbb{T}]. \end{cases}$$

It follows that

$$\Phi_{\kappa}^{\mathbf{r}}=\begin{cases}\Phi_{\kappa}(0)+\sum_{\Bbbk=2}^{\mathbf{r}}\left\{\frac{23}{12}\Upsilon(\mathbf{t}_{\Bbbk},\Phi^{\Bbbk})\Delta\mathbf{t}-\frac{4}{3}\Upsilon(\mathbf{t}_{\Bbbk-1},\Phi^{\Bbbk-1})\Delta\mathbf{t}+\frac{5}{12}\Upsilon(\mathbf{t}_{\Bbbk-2},\Phi^{\Bbbk-2})\Delta\mathbf{t}\right\}, & \mathbf{t}\in[0,\mathbb{T}_{\Bbbk}].\\ \Phi_{\kappa}(\mathbb{T}_1)+\frac{\beta}{ABC(\beta)}\Upsilon(\mathbf{t}_{n_1},\Phi^{n_1})+\frac{\beta(\Delta\mathbf{t})^{\beta-1}}{ABC(\beta)\Gamma(\beta+1)}\sum_{\Bbbk=2}^{\mathbf{r}}\Upsilon(\mathbf{t}_{\Bbbk-2},\Phi^{\Bbbk-2})\Xi_1 & \\ \quad+\frac{\beta(\Delta\mathbf{t})^{\beta-1}}{ABC(\beta)\Gamma(\beta+2)}\sum_{\Bbbk=2}^{\mathbf{r}}\left\{\Upsilon(\mathbf{t}_{\Bbbk-1},\Phi^{\Bbbk-1})-\Upsilon(\mathbf{t}_{\Bbbk-2},\Phi^{\Bbbk-2})\right\}\Xi_2 & \\ \quad+\frac{\beta(\Delta\mathbf{t})^{\beta-1}}{2ABC(\beta)\Gamma(\beta+3)}\sum_{\Bbbk=2}^{\mathbf{r}}\left\{\Upsilon(\mathbf{t}_{\Bbbk},\Phi^{\Bbbk})-2\Upsilon(\mathbf{t}_{\Bbbk-1},\Phi^{\Bbbk-1})+\Upsilon(\mathbf{t}_{\Bbbk-2},\Phi^{\Bbbk-2})\right\}\Xi_3, & \mathbf{t}\in[\mathbb{T}_1,\mathbb{T}_2],\\ \Phi_{\kappa}(\mathbb{T}_2)+\sum_{\Bbbk=\mathbf{r}+3}^{n_1}\left\{\frac{5}{12}\Upsilon(\mathbf{t}_{\Bbbk-2},\Phi^{\Bbbk-2})\Delta\mathbf{t}-\frac{4}{3}\Upsilon(\mathbf{t}_{\Bbbk-1},\Phi^{\Bbbk-1})\Delta\mathbf{t}+\frac{23}{12}\Upsilon(\mathbf{t}_{\Bbbk},\Phi^{\Bbbk})\Delta\mathbf{t}\right\} & \\ \quad+\sum_{\Bbbk=\mathbf{r}+3}^{n_1}\left\{\frac{5}{12}\big(B(\mathbf{t}_{\Bbbk-1})-B(\mathbf{t}_{\Bbbk-2})\big)\wp\Phi^{\Bbbk-2}-\frac{4}{3}\big(B(\mathbf{t}_{\Bbbk})-B(\mathbf{t}_{\Bbbk-1})\big)\wp\Phi^{\Bbbk-1}\right. & \\ \quad\left.+\frac{23}{12}\big(B(\mathbf{t}_{\Bbbk+1})-B(\mathbf{t}_{\Bbbk})\big)\wp\Phi^{\Bbbk}\right\}, & \mathbf{t}\in[\mathbb{T}_2,\mathbb{T}],\end{cases}$$

where Ξ_1, Ξ_2 and Ξ_3 are stated before in (44)–(46).

5 Results and Discussion

In this section, we will first discuss the numerical approach for the fractional model in the context of the piecewise derivatives, which is provided in [44].

As of now, the COVID-19 coronavirus infection remains among the world's deadliest and most dangerous. There is currently no therapeutic option. In addition, because of the virus's aggressive propagation and the presence of numerous unpredictable components (people's interests, mammal activities, transportation, etc.), it includes a significant amount of unpredictability. We constructed a simulation for the new 2019 coronavirus infection using stochastic concepts, and we explored the disease's propagation features and comprehended its emergence and spread in the context of community and environmental transformation via the piecewise fractional derivative operators (e.g., Caputo, Caputo-Fabrizio and Atangana-Baleanu-Caputo context). Following the implementation of the numerical approach, we will examine the physical characteristics listed in Table 1 using fractional-order β values and demonstrate the findings are mentioned below.

Table 1: List of parameters

Symbols	Explanation	Values	Sources
Λ	Recruitment rate	8972.105	Estimated
χ	Natural death rate	407300.0000	Estimated
ψ	Interaction rate	8526331000	[45]
η_1	Rate of pathogen awareness	14.11084740	[45]

(Continued)

Table 1 (continued)

Symbols	Explanation	Values	Sources
η_2	Quarantine rate	219.7398720	[45]
φ_1	Isolation rate	10.71592360	[45]
φ_2	Occurrence of clinical manifestations while quarantine	1.915503760	[45]
ζ_1	Restoration rate in affected people	1.141303480	[45]
ζ_2	Restoration rate in isolated people	27.09393550	[45]
ξ	After-treatment susceptibility rate	120.3252870	[45]
ϑ	Proportion of the confined community was isolated.	0.68	Assumed

The numerical scheme for the Caputo fractional direction indicated by (41)–(43) is studied, and the findings are schematically represented in Figs. 2–4 with lowest random intensities. Furthermore, on 7 October 2021, we might use the corresponding accurate statistics $\mathbf{S} = 220,033,703$, $\mathbf{E}(0) = 196304$, $\mathbf{Q}(0) = 32917$, $\mathbf{I}(0) = 18114$, $\mathbf{J}(0) = 0$, $\mathbf{R}(0) = 1446$ in Pakistan [45]. Then, $\mathbf{R}_0^S >, 1$ which is described in Section 3. Theorem 3.4 research shows that mechanism (41)–(43) will exist for a long period due to a distribution $\pi(.)$ This is supported by numerical simulations (Figs. 2–4). In particular, considering Pakistani statistical information from October to December 2021, the estimate (Figs. 2–4) shows that controlling the isolation level will influence the perturbation of the prevalence of disease and regulate the growth in the infected population. Simultaneously, when the transmission incidence is disrupted by several other variables, including vaccine administration, the death toll reduces along with the amount of infections. This is essentially in accordance with the system's (41)–(43) study findings in this work.

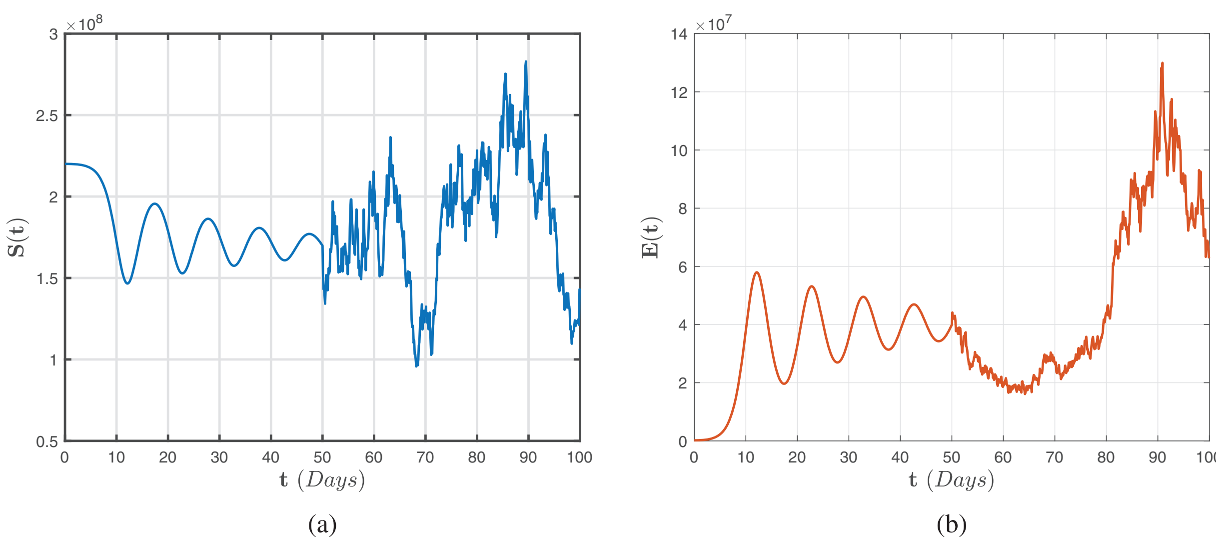

Figure 2: Numerical representations for the model (41)–(43) for the susceptible $\mathbf{S}(\mathbf{t})$ and exposed $\mathbf{E}(\mathbf{t})$ individuals when random densities $\wp_1 = 0.05, \wp_2 = 0.06, \wp_3 = 0.07, \wp_4 = 0.08, \wp_5 = 0.09$ and $\wp_1 = 0.09$ via the Caputo derivative operator with fractional-order assumed to be 0.95

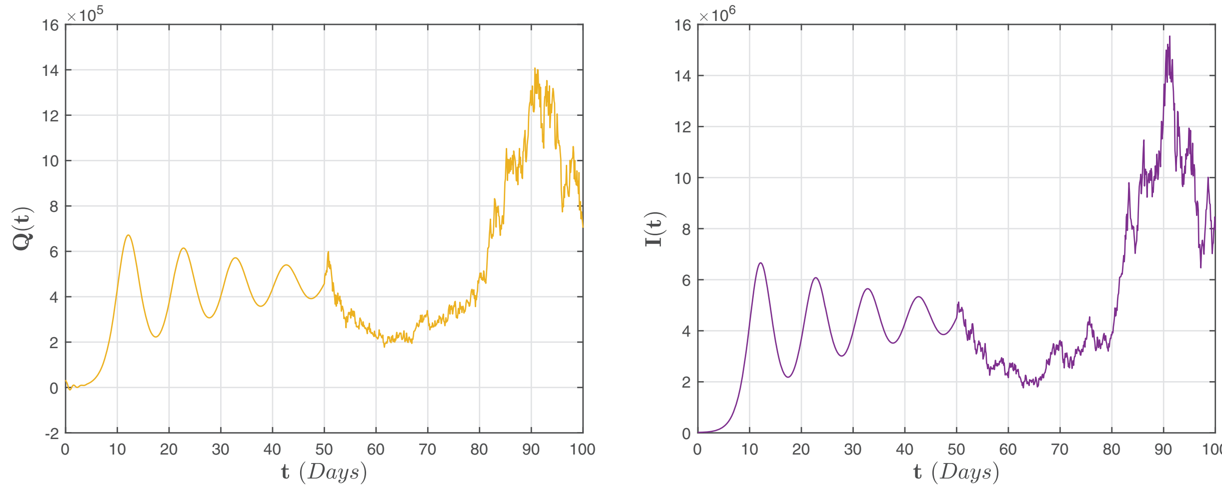

(a) (b)

Figure 3: Numerical representations for the model (41)–(43) for the quarantined $\mathbf{Q}(\mathbf{t})$ and infected $\mathbf{I}(\mathbf{t})$ individuals when random densities $\wp_1 = 0.05, \wp_2 = 0.06, \wp_3 = 0.07, \wp_4 = 0.08, \wp_5 = 0.09$ and $\wp_1 = 0.09$ via the Caputo derivative operator with fractional-order assumed to be 0.95

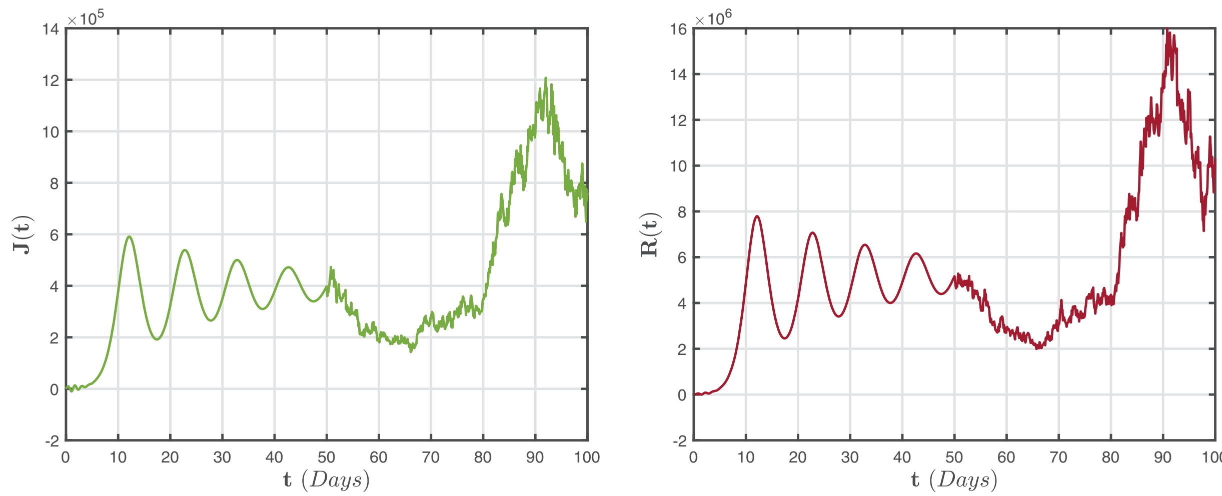

(a) (b)

Figure 4: Numerical representations for the model (41)–(43) for the isolated $\mathbf{J}(\mathbf{t})$ and recovered $\mathbf{R}(\mathbf{t})$ individuals when random densities $\wp_1 = 0.05, \wp_2 = 0.06, \wp_3 = 0.07, \wp_4 = 0.08, \wp_5 = 0.09$ and $\wp_1 = 0.09$ via the Caputo derivative operator with fractional-order assumed to be 0.95

Figs. 5–7 illustrates numerical findings for the Caputo-Fabrizio sense for (47)–(49) by utilizing environmental noise values. Furthermore, the performance parameters state the biological suitability of the finding. Following that, we shall concentrate on the stochastic simulation analysis (47)–(49). Figs. 5–7 depicts the trajectories of $\mathbf{I}(\mathbf{t})$ and $\mathbf{R}(\mathbf{t})$ in various scenarios. We can observe that the stochastic model's solution varies within underlying deterministic model, demonstrating how noise can influence the quantity of individuals afflicted and eliminated. To clearly demonstrate the impact of noise, we present in Fig. 5b the path of $\mathbf{I}(\mathbf{t})$ for the stochastic process (47)–(49) having various noise concentrations as well as its associated deterministic structure. Furthermore, in Fig. 7b, we depict the variation of the mean value of each time in the 5000 pathways of the stochastic process (47)–(49) plus or minus the standard deviation in Fig. 7b. It has been discovered that the greater the noise concentration $\wp_6 = 0.09$, the deeper the volatility of $\mathbf{I}(\mathbf{t})$. It can also be shown that as the noise levels increase, the standard deviation of $\mathbf{I}(\mathbf{t})$ grows and its average value decreases $\wp_6 = 0.09$, indicating that the disturbance has crossover deterministic-stochastic patterns and can prevent illness transmission.

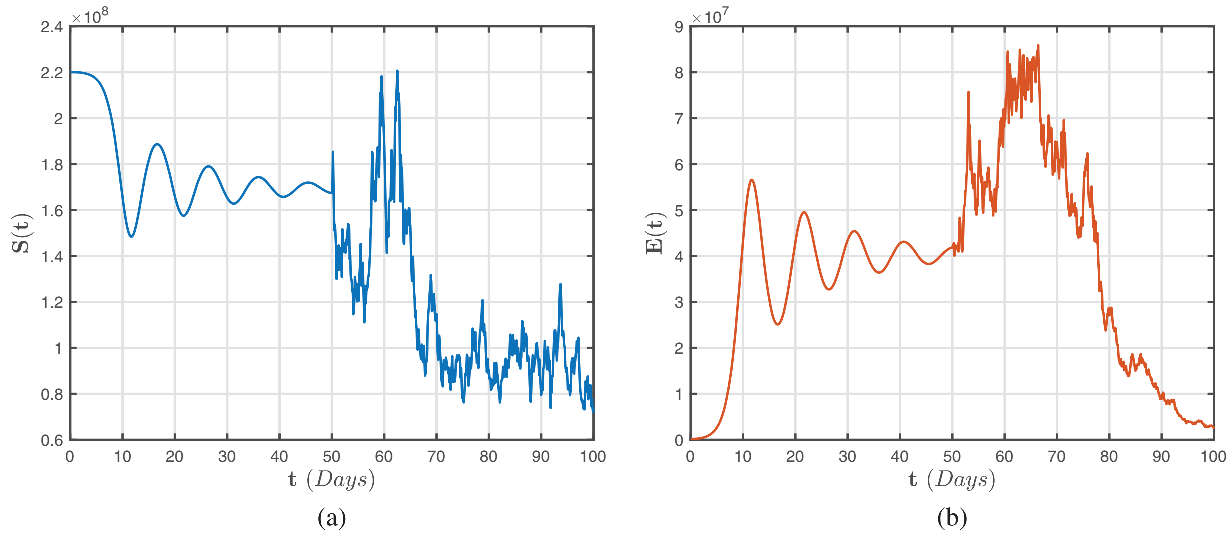

Figure 5: Numerical representations for the model (47)–(49) for the susceptible $\mathbf{S}(\mathbf{t})$ and exposed $\mathbf{E}(\mathbf{t})$ individuals when random densities $\wp_1 = 0.05, \wp_2 = 0.06, \wp_3 = 0.07, \wp_4 = 0.08, \wp_5 = 0.09$ and $\wp_1 = 0.09$ via the Caputo-Fabrizio derivative operator with fractional-order assumed to be 0.95

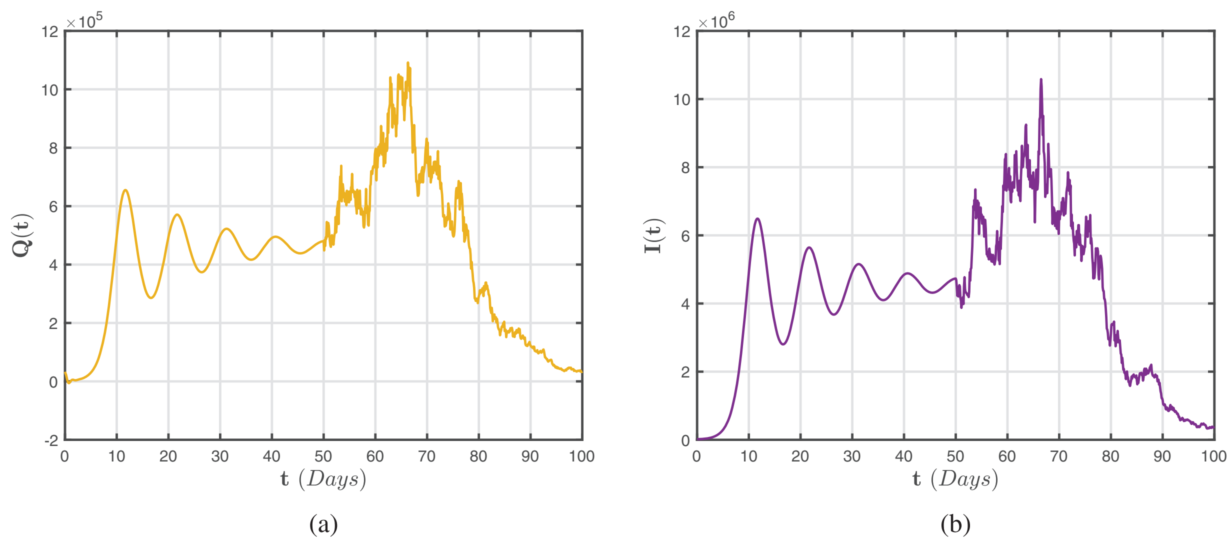

Figure 6: Numerical representations for the model (47)–(49) for the quarantined $\mathbf{Q}(\mathbf{t})$ and infected $\mathbf{I}(\mathbf{t})$ individuals when random densities $\wp_1 = 0.05, \wp_2 = 0.06, \wp_3 = 0.07, \wp_4 = 0.08, \wp_5 = 0.09$ and $\wp_1 = 0.09$ via the Caputo-Fabrizio derivative operator with fractional-order assumed to be 0.95

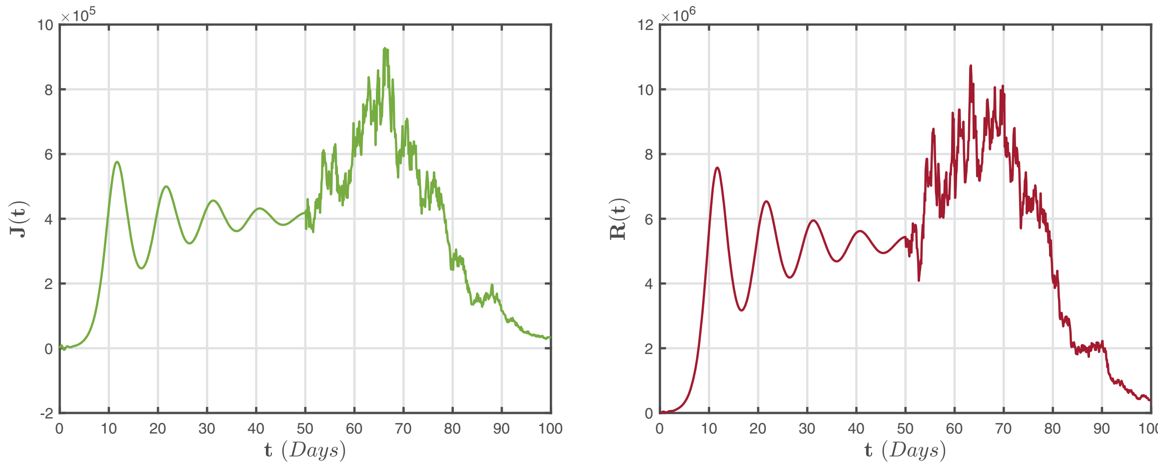

(a) (b)

Figure 7: Numerical representations for the model (47)–(49) for the isolated $\mathbf{J}(\mathbf{t})$ and recovered $\mathbf{R}(\mathbf{t})$ individuals when random densities $\wp_1 = 0.05, \wp_2 = 0.06, \wp_3 = 0.07, \wp_4 = 0.08, \wp_5 = 0.09$ and $\wp_1 = 0.09$ via the Caputo-Fabrizio derivative operator with fractional-order assumed to be 0.95

Analogously, Figs. 8–10 illustrate numerical findings for the Atangana-Baleanu-Caputo sense for (52)–(54) by utilizing environmental noise values. In particular, it may be stated that increased noise $\wp_3$ will be useful in reducing the number of contaminated people $\mathbf{I}(\mathbf{t})$ on average. As a result, we can suitably raise the volume of noise to prevent the transmission of the disease. The preceding scenario indicates that randomized disruptions may minimize the incidence of viruses. One will immediately recognise that several of them display crossover tendencies, such as a crossover from deterministic to stochastic processes.

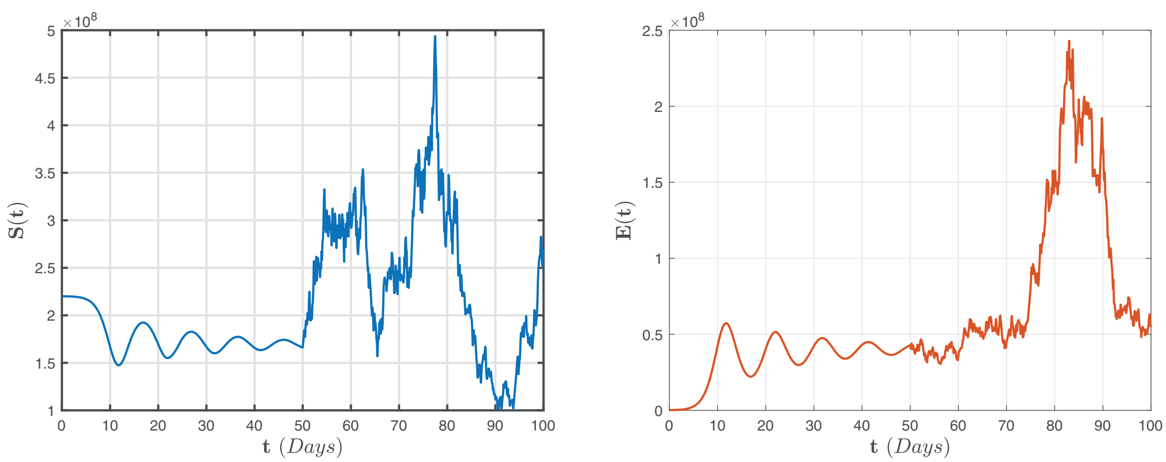

(a) (b)

Figure 8: Numerical representations for the model (52)–(54) for the susceptible $\mathbf{S}(\mathbf{t})$ and exposed $\mathbf{E}(\mathbf{t})$ individuals when random densities $\wp_1 = 0.05, \wp_2 = 0.06, \wp_3 = 0.07, \wp_4 = 0.08, \wp_5 = 0.09$ and $\wp_1 = 0.09$ via the Atangana-Baleanu-Caputo derivative operator with fractional-order assumed to be 0.95

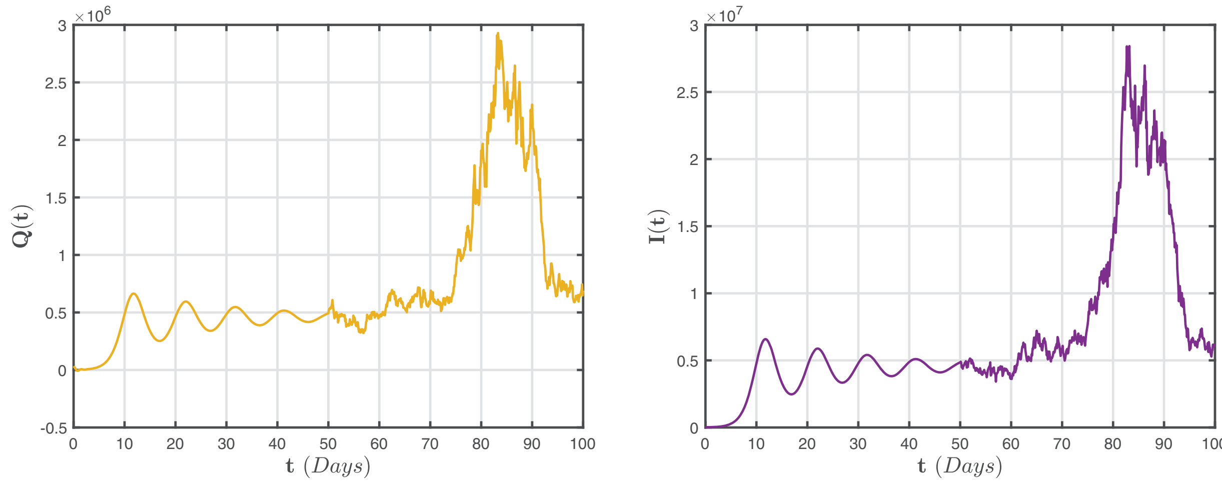

(a) (b)

Figure 9: Numerical representations for the model (52)–(54) for the quarantined $\mathbf{Q}(\mathbf{t})$ and infected $\mathbf{I}(\mathbf{t})$ individuals when random densities $\wp_1 = 0.05, \wp_2 = 0.06, \wp_3 = 0.07, \wp_4 = 0.08, \wp_5 = 0.09$ and $\wp_1 = 0.09$ via the Atangana-Baleanu-Caputo derivative operator with fractional-order assumed to be 0.95

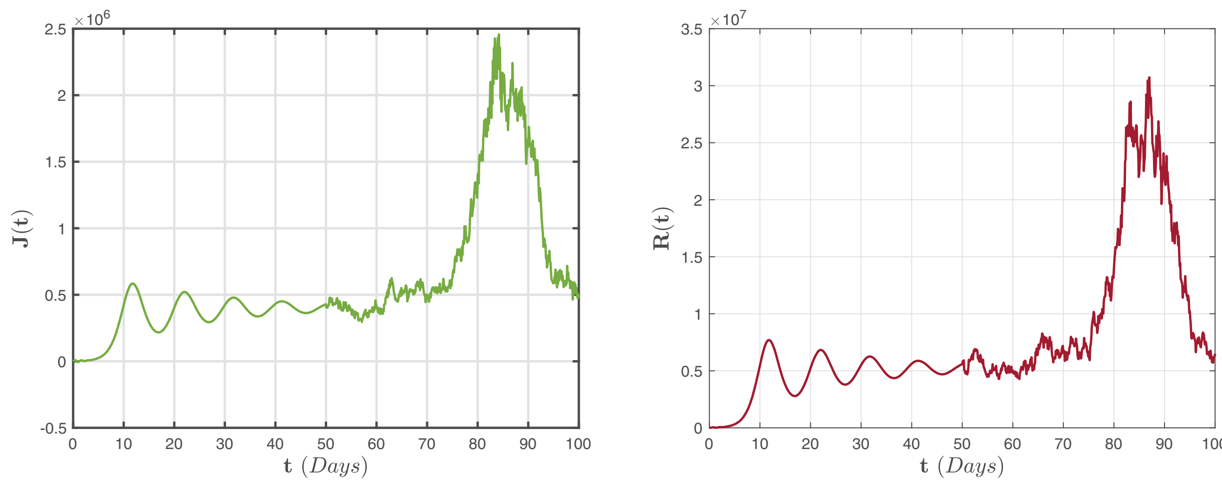

(a) (b)

Figure 10: Numerical representations for the model (52)–(54) for the isolated $\mathbf{J}(\mathbf{t})$ and recovered $\mathbf{R}(\mathbf{t})$ individuals when random densities $\wp_1 = 0.05, \wp_2 = 0.06, \wp_3 = 0.07, \wp_4 = 0.08, \wp_5 = 0.09$ and $\wp_1 = 0.09$ via the Atangana-Baleanu-Caputo derivative operator with fractional-order assumed to be 0.95

Figs. 11–13 show the chaotic behaviour of the model (52)–(54) with varying random intensities and fixed fractional-order $\beta = 0.95$. According to the aforementioned evaluation, boosting isolation and quarantine and raising the efficacy of the treatment can significantly decrease the population of affected patients; consequently, rigorous prevention and confinement techniques are required. The number of affected people diminishes to a certain level as η_2 climbs and declines ψ. This signifies that adopting proper utilization press attention raises people's awareness of the importance of taking proper precautions, which can improve the lowered interaction rate as a consequence of press attention, thereby assisting to reduce the severity of transmission by indicating that the disturbance has crossover deterministic-stochastic patterns.

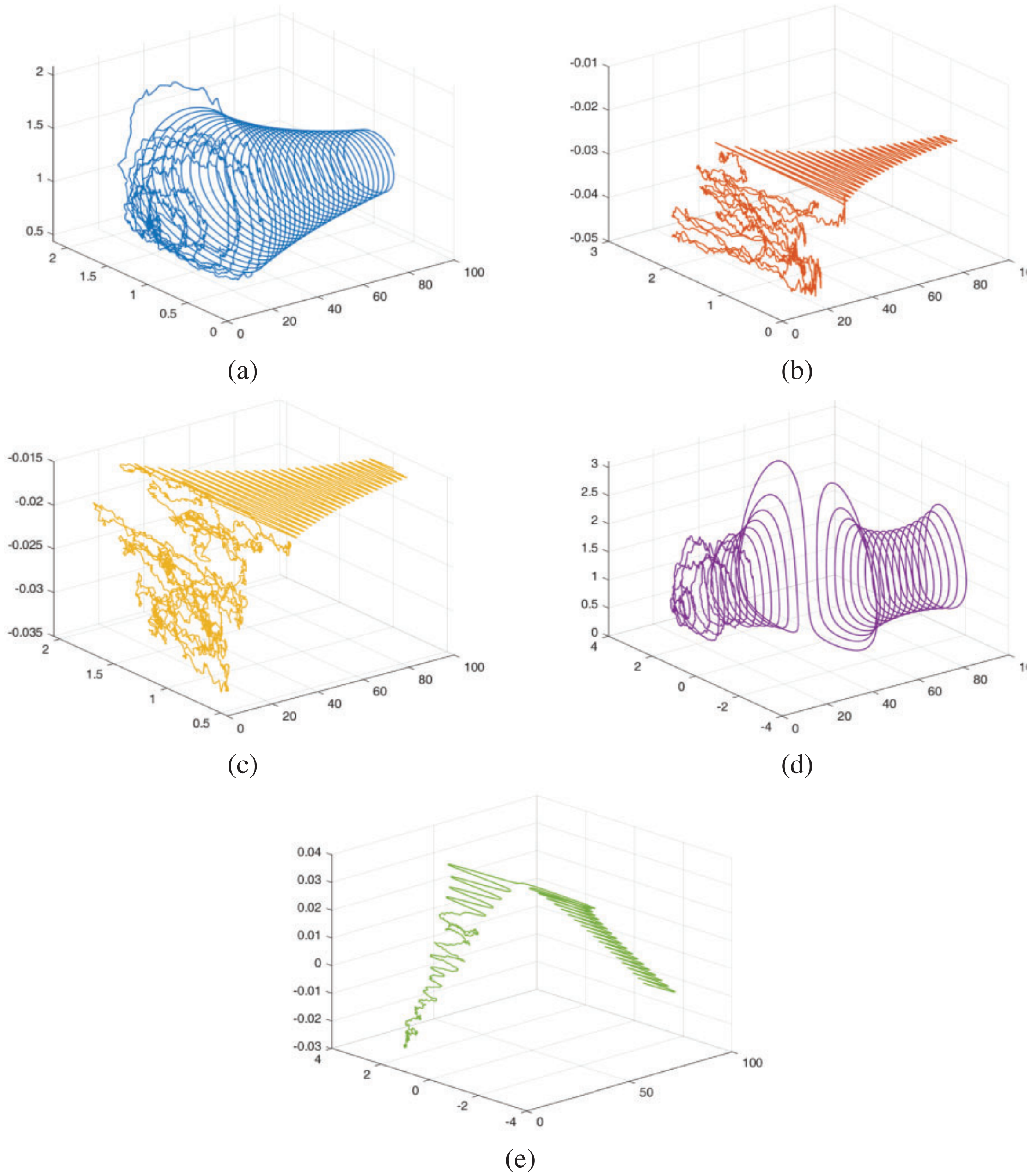

Figure 11: The dynamical behaviour of the model (52)–(54) for various cohorts when random densities $\wp_1 = 0.05, \wp_2 = 0.06, \wp_3 = 0.07, \wp_4 = 0.08, \wp_5 = 0.09$ and $\wp_1 = 0.09$ via the Atangana-Baleanu-Caputo derivative operator with fractional-order assumed to be 0.95

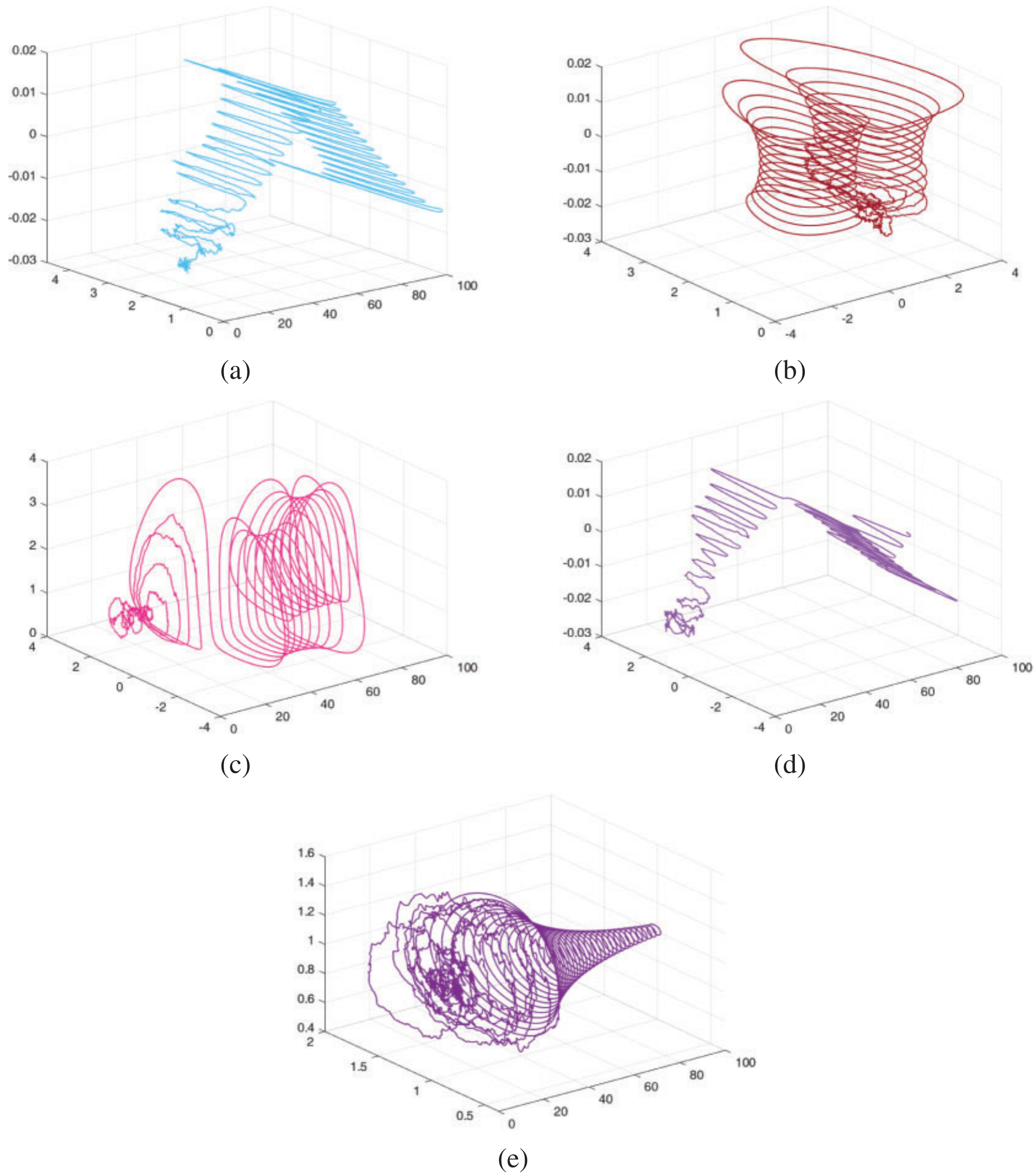

Figure 12: The dynamical behaviour of the model (52)–(54) for various cohorts when random densities $\wp_1 = 0.05, \wp_2 = 0.06, \wp_3 = 0.07, \wp_4 = 0.08, \wp_5 = 0.09$ and $\wp_1 = 0.09$ via the Atangana-Baleanu-Caputo derivative operator with fractional-order assumed to be 0.95

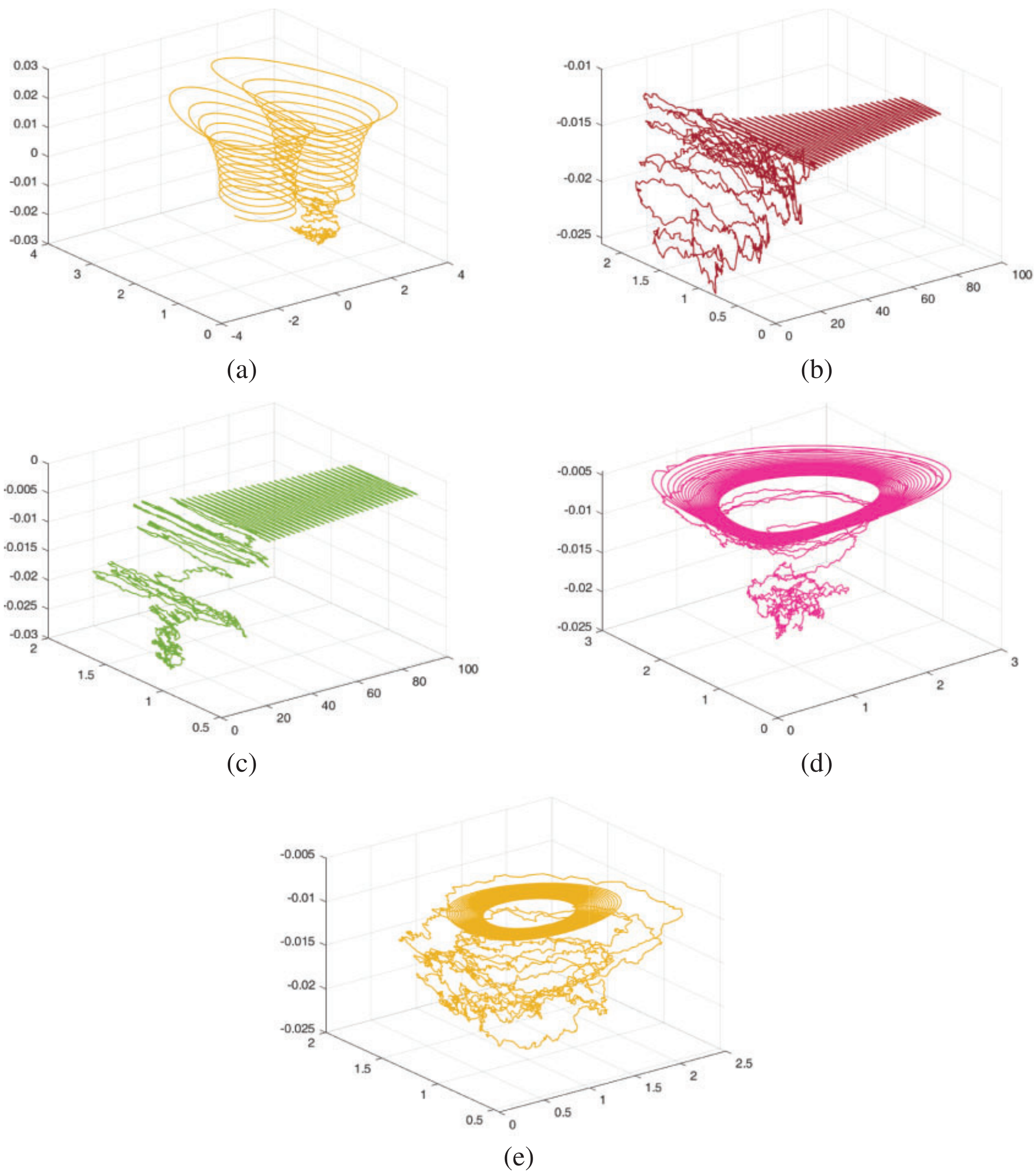

Figure 13: The dynamical behaviour of the model (52)–(54) for various cohorts when random densities $\wp_1 = 0.05, \wp_2 = 0.06, \wp_3 = 0.07, \wp_4 = 0.08, \wp_5 = 0.09$ and $\wp_1 = 0.09$ via the Atangana-Baleanu-Caputo derivative operator with fractional-order assumed to be 0.95

6 Conclusion

Contemporary research proposes a comprehensive framework for the existing coronavirus epidemic, including a particular emphasis on the interactions of quarantined, infected, and isolated groups via crossover behaviours. For the deterministic system, we establish the strength number. In the associated stochastic process, we first determine the extinction and permanence thresholds, followed by the ergodic stationary distribution. Even though considerable and extremely interesting outcomes have been proposed, when glancing at the transmission of COVID-19, particularly documentation from a country, someone could immediately discover that several of them exemplify crossover behaviours, such as a transition from configurations to deterministic functionalities to structures to stochastic capabilities. Employing the approach of piecewise modelling, we aimed to offer a novel aperture for modelling analogous issues. We include several illustrations to demonstrate our point. The concordance between the piecewise estimates and experimental evidence demonstrates without a dispute that this technique will aid humans in accurately predicting crossover behaviours in evolutionary biology.

Acknowledgement: The researchers would like to acknowledge Deanship of Scientific Research, Taif University for funding this work.

Funding Statement: The authors received no specific funding for this study.

Conflicts of Interest: The authors declare that they have no conflicts of interest to report regarding the present study.

References

1. World Health Organization (2020). Who.int/csr/don/12-january-2020-novelcoronavirus-china
2. Kouidere, A., Youssoufi, L. E., Ferjouchia, H., Balatif, O., Rachik, M. (2021). Optimal control of mathematical modeling of the spread of the COVID-19 pandemic with highlighting the negative impact of quarantine on diabetics people with cost-effectiveness. *Chaos, Solitons and Fractals, 145(3),* 110777.
3. Das, M., Samanta, G. (2021). Stability analysis of a fractional ordered COVID-19 model. *Computational and Mathematical Biophysics, 9(1),* 22–45.
4. Pacurar, C. M., Necula, B. R. (2020). An analysis of COVID-19 spread based on fractal interpolation and fractal dimension. *Chaos, Solitons and Fractals, 139(3),* 8.
5. Zhang, Z. (2020). Corrigendum to a novel COVID-19 mathematical model with fractional derivatives: Singular and nonsingular kernels. *Chaos, Solitons and Fractals, 139(2),* 110128.
6. Begum, R., Tunc, O., Khan, H., Gulzar, H., Khan, A. (2021). A fractional order Zika virus model with Mittag-Leffler kernel. *Chaos, Solitons and Fractals, 146(2),* 11.
7. He, Z. Y., Abbes, A., Jahanshahi, H., Alotaibi, N. D., Wang, Y. (2022). Fractional-order discrete-time SIR epidemic model with vaccination: Chaos and complexity. *Mathematics, 10(2),* 165. https://doi.org/10.3390/math10020165
8. Jin, F., Qian, Z. S., Chu, Y. M., Rahman, M. (2022). On nonlinear evolution model for drinking behavior under Caputo-Fabrizio derivative. *Journal of Applied Analysis & Computation, 12(2),* 790–806.
9. Wang, F. Z., Khan, M. N., Ahmad, I., Ahmad, H., Abu-Zinadah, H. et al. (2022). Numerical solution of traveling waves in chemical kinetics: Time-fractional Fishers equations. *Fractals, 30(2),* 22400051. https://doi.org/10.1142/S0218348X22400515
10. Dehingia, K., Yao, S. W., Sadri, K., Das, A., Kumar, H. S. et al. (2022). A study on cancer-obesity-treatment model with quadratic optimal control approach for better outcomes. *Results in Physics, 42(1),* 105963.
11. Partohaghighi, M., Veeresha, P., Akgül, A., Inc, M., Riaz, M. B. (2022). Fractional study of a novel hyper-chaotic model involving single non-linearity. *Results in Physics, 42(1),* 105965.
12. Zafar, Z. A., Hussain, M. T., Inc, M., Baleanu, D., Almohsenh, B. et al. (2022). Fractional-order dynamics of human papillomavirus. *Results in Physics, 34(3),* 105281.
13. Acay, B., Inc, M., Mustapha, U. T., Yusuf, A. (2021). Fractional dynamics and analysis for a lana fever infectious ailment with Caputo operator. *Chaos, Soliton and Fractals, 153(3),* 111605.

14. Rihan, F. A., Alsakaji, H. J. (2021). Dynamics of a stochastic delay differential model for COVID-19 infection with asymptomatic infected and interacting peoples: A case study in the UAE. *Results in Physics, 28(5),* 104658. https://doi.org/10.1016/j.rinp.2021.104658
15. Tang, B., Wang, X., Li, Q., Bragazzi, N. L., Tang, S. et al. (2020). Estimation of the transmission risk of the 2019-nCoVand its implication for public health interventions. *Journal of Clinical Medicine, 9(2),* 462–474. https://doi.org/10.3390/jcm9020462
16. Tang, B., Bragazzi, N. L., Li, Q., Tang, S., Xiao, Y. et al. (2020). An updated estimation of the risk of transmission of the novel coronavirus (2019-nCoV). *Infectious Diseases Modelling, 5(7),* 248–255. https://doi.org/10.1016/j.idm.2020.02.001
17. Li, Y., Wang, B., Peng, R., Zhou, C., Zhan, Y. et al. (2020). Mathematical modeling and epidemic prediction of COVID-19 and its significance to epidemic prevention and control measures. *Journal of Current Scientific Research, 1(1),* 19–36.
18. Qianying, L., Zhao, S., Gao, D., Lou, Y., Yang, S. et al. (2020). A conceptual model for the coronavirus disease 2019 (COVID-19) outbreak in Wuhan, China with individual reaction and governmental action. *International Journal of Infectious Diseases, 93(1766),* 211–216. https://doi.org/10.1016/j.ijid.2020.02.058
19. Khan, M. A., Atangana, A. (2020). Modeling the dynamics of novel coronavirus (2019-nCoV) with fractional derivative. *Alexandria Engineering Journal, 59(4),* 2379–2389.
20. Ivorra, B., Ferrández, M. R., Vela-Pérez, M., Ramos, A. M. (2020). Mathematical modeling of the spread of the coronavirus disease 2019 (COVID-19) considering its particular characteristics. The case of China. *Communications in Nonlinear Science and Numerical Simulation, 88(1),* 105303. https://doi.org/10.1016/j.cnsns.2020.105303
21. Alsakaji, H. J., Rihan, F. A., Hashish, A. (2022). Dynamics of a stochastic epidemic model with vaccination and multiple time-delays for COVID-19 in the UAE. *Complexity, 2022,* 1–15.
22. Zhao, T. H., Castillo, O., Jahanshahi, H., Yusuf, A., Alassafi, M. O. et al. (2021). A fuzzy-based strategy to suppress the novel coronavirus (2019-nCoV) massive outbreak. *Applied and Computational Mathematics, 20,* 160–176.
23. Baba, I. A., Rihan, F. A. (2022). A fractional-order model with different strains of COVID-19. *Physica A, 603,* 127813.
24. Fadaei, Y., Rihan, F. A., Rajivganthi, C. (2022). Immunokinetic model for COVID-19 patients. *Complexity, 2022(1),* 8321848. https://doi.org/10.1155/2022/8321848
25. Nazeer, M., Hussain, F., Ijaz, K. M., Rehman, A., El-Zahar, E. R. et al. (2021). Theoretical study of MHD electro-osmotically flow of third-grade fluid in micro channel. *Applied and Computational Mathematics, 420(2),* 126868. https://doi.org/10.1016/j.amc.2021.126868
26. Chu, Y. M., Shankaralingappa, B. M., Gireesha, B. J., Alzahrani, F., Khan, M. I. et al. (2021). Combined impact of Cattaneo-Christov double diffusion and radiative heat flux on bio-convective flow of Maxwell liquid configured by a stretched nano-material surface. *Applied and Computational Mathematics, 419(1),* 126883. https://doi.org/10.1016/j.amc.2021.126883
27. Zhao, T. H., Khan, M. I., Chu, Y. M. (2021). Artificial neural networking (ANN) analysis for heat and entropy generation in flow of non-Newtonian fluid between two rotating disks. *Mathematical Methods in Applied Sciences, 46(3),* 3012–3030. https://doi.org/10.1002/mma.7310
28. Caputo, M. (1967). Linear model of dissipation whose Q is almost frequency independent II. *Geophysical Journal International, 13(5),* 529–539.
29. Rashid, S., Abouelmagd, E. I., Sultana, S., Chu, Y. M. (2022). New developments in weighted n-fold type inequalities via discrete generalized $\hat{h}$-proportional fractional operators. *Fractals, 30(2),* 2240056. https://doi.org/10.1142/S0218348X22400564
30. Rashid, S., Sultana, S., Karaca, Y., Khalid, A., Chu, Y. M. (2022). Some further extensions considering discrete proportional fractional operators. *Fractals, 30(1),* 2240026.

31. Rashid, S., Abouelmagd, E. I., Khalid, A., Farooq, F. B., Chu, Y. M. (2022). Some recent developments on dynamical h-discrete fractional type inequalities in the frame of nonsingular and nonlocal kernels. *Fractals, 30(2),* 2240110.
32. Erturk, V. S., Godweb, E., Baleanu, D., Kumar, P., Asad, J. et al. (2021). Novel fractional-order Lagrangian to describe motion of beam on nanowire. *Acta Physica Polonica Series, 140,* 265–272. https://doi.org/10.12693/APhysPolA.140.265
33. Viera-Martin, E., Gómez-Aguilar, J. F., Solís-Pérez, J. E., Hernández-Pérez, J. A., Escobar-Jiménez, R. F. (2022). Artificial neural networks: A practical review of applications involving fractional calculus. *The European Physical Journal Special Topics, 231(10),* 2059–2095.
34. Prabhakar, T. R. (1971). A singular integral equation with a generalized Mittag-LeÂ er function in the kernel. *Yokohama Mathematical Journal, 19(1),* 171–183.
35. Iqbal, M. A., Wang, Y., Miah, M. M., Osman, M. S. (2022). Study on date-Jimbo-Kashiwara-Miwa equation with conformable derivative dependent on time parameter to find the exact dynamic wave solutions. *Fractal and Fractional, 6(1),* 4. https://doi.org/10.3390/fractalfract6010004
36. Chu, Y. M., Nazir, U., Sohail, M., Selim, M. M., Lee, J. R. (2021). Enhancement in thermal energy and solute particles using hybrid nanoparticles by engaging activation energy and chemical reaction over a parabolic surface via finite element approach. *Fractal and Fractional, 5(3),* 119. https://doi.org/10.3390/fractalfract5030119
37. Karthikeyan, K., Karthikeyan, P., Baskonus, H. M., Venkatachalam, K., Chu, Y. M. (2021). Almost sectorial operators on Ψ-Hilfer derivative fractional impulsive integro-differential equations. *Mathematical Methods in Applied Sciences, 45(13),* 8045–8059. https://doi.org/10.1002/mma.7954
38. Hajiseyedazizi, S. N., Samei, M. E., Alzabut, J., Chu, Y. M. (2019). On multi-step methods for singular fractional q-integro-differential equations. *Open Mathematics, 19(1),* 1378–1405. https://doi.org/10.1515/math-2021-0093
39. Caputo, M., Fabrizio, M. (2015). A new definition of fractional derivative without singular kernel. *Progress in Fractional Differentiation and Applications, 1(2),* 73–85.
40. Atangana, A., Baleanu, D. (2016). New fractional derivatives with non-local and non-singular kernel: Theory and application to heat transfer model. *Thermal Science, 2,* 763–769.
41. Sabatier, J. (2020). Fractional-order derivatives defined by continuous kernels: Are they really too restrictive? *Fractal and Fractional, 4(3),* 40.
42. Wu, G. C., Deng, Z. G., Baleanu, D., Zeng, D. Q. (2019). New variable-order fractional chaotic systems for fast image encryption. *Chaos, 29(8),* 083103.
43. Atangana, A., Igrt, A. S. (2021). New concept in calculus: Piecewise differential and integral operators. *Chaos, Soliton and Fractals, 145(2),* 110638.
44. Atangana, A., Araz, S. I. (2021). Modeling third waves of COVID-19 spread with piecewise differential and integral operators: Turkey, Spain and Czechia. *Results in Physics, 29(2),* 104694.
45. Memona, Z., Qureshi, S., Memon, B. R. (2021). Assessing the role of quarantine and isolation as control strategies for COVID-19 outbreak: A case study. *Chaos, Solitons and Fractals, 144,* 110655.
46. Zeb, A., Alzahrani, E., Erturk, V. S., Zaman, G. (2020). Mathematical model for coronavirus disease 2019 (COVID-19) containing isolation class. *Biomedical Research International, 2020,* 1–7. https://doi.org/10.1155/2020/3452402
47. Rihan, F. A., Alsakaji, H. J. (2021). Analysis of a stochastic HBV infection model with delayed immune response. *Mathematical Biosciences in Engineering, 18(5),* 5194–5220. https://doi.org/10.3934/mbe.2021264
48. Rashid, S., Iqbal, M. K., Alshehri, A. M., Ashraf, R., Jarad, F. (2022). A comprehensive analysis of the stochastic fractal-fractional tuberculosis model via Mittag-Leffler kernel and white noise. *Results in Physics, 39(5),* 105764. https://doi.org/10.1016/j.rinp.2022.105764

49. Atangana, A., Araz, S. I. (2022). Deterministic-Stochastic modeling: A new direction in modeling real world problems with crossover effect. *Mathematical Biosciences in Engineering, 19,* 3526–3563. https://doi.org/10.3934/mbe.2022163
50. Rashid, S., Ashraf, R., Asif, Q. A., Jarad, F. (2022). Novel stochastic dynamics of a fractal-fractional immune effector response to viral infection via latently infectious tissues. *Mathematical Biosciences in Engineering, 19(11),* 11563–11594. https://doi.org/10.3934/mbe.2022539
51. Oksendal, B. (2003). *Stochastic differential equations: An introduction with applications*, 6th edition. New York, NY, USA: Springer.
52. Atangana, A. (2021). Mathematical model of survival of fractional calculus, critics and their impact: How singular is our world? *Advances in Difference Equations, 2021(1),* 1–59. https://doi.org/10.1186/s13662-021-03494-7
53. Driessche, P., Watmough, J. (2002). Reproduction numbers and sub-threshold endemic equilibria for compartmental models of disease transmission. *Mathematical Biosciences in Engineering, 180(1–2),* 29–48.
54. Mao, X. (1997). *Stochastic differential equations and applications*. Chichester: Horwood Publishing.
55. Mao, X., Marion, G., Renshaw, E. (2002). Environmental Brownian noise suppresses explosions in population dynamics. *Stochastic Process and Applications, 97(1),* 95–110.
56. Lipster, R. (1980). A strong law of large numbers for local martingales. *Stochastics, 3(1–4),* 217–228.
57. Hasminiskii, R. (1980). Stochastic stability of differential equations. In: *Stochastic Modelling and Applied Probability,* vol. 66. https://doi.org/10.1007/978-3-642-23280-0
58. Ji, C., Jiang, D. (2014). Treshold behaviour of a stochastic SIR model. *Applied Mathematical Modelling, 38(21–22),* 5067–5079. https://doi.org/10.1016/j.apm.2014.03.037